Computer Model Verification and Testing of an

Apricus AP-30 Evacuated Tube Collector Array

by

Matthew Stonebraker

A Thesis Presented in Partial Fulfillment
of the Requirements for the Degree
Master of Science

Approved November 2011 by the
Graduate Supervisory Committee:

Patrick Phelan, Chair
T Agami Reddy
Harvey Bryan

ARIZONA STATE UNIVERSITY

December 2011

ABSTRACT

Evacuated tube solar thermal collector arrays have a wide range of applications. While most of these applications are limited in performance due to relatively low maximum operating temperatures, these collectors can still be useful in low grade thermal systems. An array of fifteen Apricus AP-30 evacuated tube collectors was designed, assembled, and tested on the Arizona State University campus in Tempe, AZ. An existing system model was reprogrammed and updated for increased flexibility and ease of use. The model predicts the outlet temperature of the collector array based on the specified environmental conditions. The model was verified through a comparative analysis to the data collected during a three-month test period. The accuracy of this model was then compared against data calculated from the Solar Rating and Certification Corporation (SRCC) efficiency curve to determine the relative performance. It was found that both the original and updated models were able to generate reasonable predictions of the performance of the collector array with overall average percentage errors of 1.0% and 1.8%, respectively.

DEDICATION

This thesis is dedicated to my wife Isabelle. Without your constant support and patience, this would not have been possible. I appreciate everything you have done to make this process easier on me. Thank you and I love you.

ACKNOWLEDGMENTS

TABLE OF CONTENTS

LIST OF TABLES

LIST OF FIGURES

LIST OF SYMBOLS / NOMENCLATURE

A	area (m^2)
C_p	specific heat capacity ($^J/_{kg\,K}$)
F_R	collector heat removal factor
F'	collector efficiency factor
I	incident solar radiation (W/m^2)
I_o	incident solar radiation on a horizontal surface (W/m^2)
L_s	thermal load on collector storage tank (W)
m	mass (kg)
$\dot{m}$	mass flow rate (kg/s)
Q_u	useful heat gain (W)
R	resistance
R_b	ratio of beam to horizontal radiation
S	absorbed solar radiation (W)
T	temperature (°C, K)
U_L	overall heat transfer coefficient (W/m^2 K)
U	thermal loss coefficient (W/m^2 K)
V	volume (gallons, liters)
X	Thermal Expansion Ratio

Greek Symbols

β	coefficient of thermal expansion (1/K)
η	efficiency
ρ	reflectance

Subscripts

a	ambient
b	beam
c	Carnot
d	diffuse
f	fluid
gr	ground
hp	heat pipe
i	inlet
k	condenser
ma	manifold
o	outlet
rad	radiative
s	storage tank

CHAPTER 1

INTRODUCTION

1.1 – Overview and Motivation

The study and application of solar energy is not a new practice. As early as the 7th century B.C., people were using the combination of a magnifying glass with the sun to start fires [1]. However, enthusiasm in the development of solar-based technologies has come into and out of vogue throughout its long history. Recently, the rising price of fossil fuels combined with their quickly decreasing supply has led to the realization that the current energy system is not sustainable. This has led to a shift in focus toward the development of renewable energy sources. Some of the most promising technologies in renewable energy production are solar photovoltaic and solar thermal systems. The flexibility and relative ease by which solar thermal collectors can be manufactured has made them a very attractive renewable energy solution.

There are essentially two categories of solar thermal collectors: non-concentrating and concentrating. Concentrating collectors use reflective surfaces to direct sunlight toward a small absorbing point while non-concentrating collectors directly expose the absorber to solar radiation. Selection of a collector type is ultimately based on the temperature requirements of the intended use. A table depicting the different types of collectors with their heliostatic tracking requirements and their normal operating temperatures can be seen in Appendix A. [2]

Solar thermal collectors can be used in a wide range of applications such as water heating, refrigeration, and steam generation for electricity production. Moving forward, the proper design and application of these collectors can make a

1

major contribution in the shift away from fossil fuel dependency. Greater understanding and more accurate predictive models of collector output will supply the much needed knowledge to develop successful solar arrays with consistent and sustainable energy production.

1.2 - Objective

The following investigation is designed to refine and update a predictive model, originally designed by Witt [3], used to study the Apricus AP-30 evacuated tube (EVT) collector. This model is then tested and validated by setting up and operating an array of fifteen Apricus AP-30 collectors. Ultimately these collectors will serve as the heat source for a "thermal hydraulic" engine. This engine, named the Deluge Natural Energy Engine (DNEE) [4], is subsequently used to replace the electric refrigerant compressor of a standard ten-ton air conditioning system. Fig. 1 shows a general schematic of the DNEE refrigeration system. Further information on the integration of the DNEE into the refrigeration system can be seen in section 2.4.
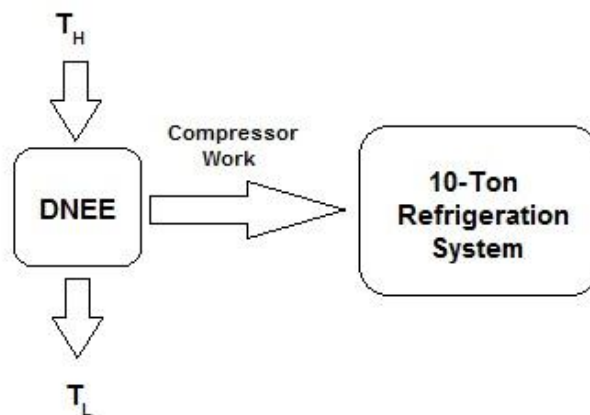
Figure 1. General schematic of the DNEE refrigeration system.

The DNEE used in this project was designed and built by Deluge Inc., therefore little focus will be spent on the design of this engine. The majority of the analysis presented here will describe the computer modeling, installation, and testing of the solar thermal array. The computer model, originally developed by Witt [3], will be reviewed and improved upon to generate more accurate predictions of the EVT performance. The layout of the solar collectors combines manufacturer recommendations with simple engineering calculations to optimize the effectiveness of the system.

The primary goal of this study is to install and test an EVT collector array. The computer model, which will be used to predict the amount of energy transferred to the working fluid, will be validated by a comparison with experimental results generated from this array.

1.3 – Literature Review

Currently, there are several methods of generating refrigeration using solar thermal energy. These methods include solar absorption [5,6], solar adsorption [6], and the combination of a Rankine cycle engine and conventional refrigeration system [7,8,9,10]. These refrigeration systems have the capability of operating at surprisingly low temperatures. In fact, in most cases, the input temperature can be achieved with non-tracking collectors [5].

There have been many investigations done on developing models to predict the performance of stationary collectors. In a 2009 study conducted by Villar et. al. [11], a transient 3-D model was developed for flat plate collectors. This model was capable of comparing several different configurations such as parallel tube collectors, serpentine tube collectors, two parallel plate collectors, along with other unusual combinations. Once developed, the model was

validated using experimental data for commercial parallel tube collectors [11]. Selmi et. al. [12] used a similar method in their analysis of flat plate collectors. They also generated a 3-D model and used CFD software to calculate temperatures in the system. A very in-depth temperature distribution on the cross section of the collector was generated for different operating conditions, and the predicted fluid outlet temperature of the collector was compared to experimental results to validate the simulation [12]. Other interesting methods used to model flat plate collectors included using artificial neural networks [13], using the Discrete Transfer Radiation Model [14], and creating a 1-D transient mathematical model [15].

Thorough investigations into the modeling and testing of evacuated tube (EVT) collectors have also been conducted. Budihardjo and Morrison created a model to predict the performance of evacuated tube collectors using the TRNSYS program in 2008. The collector design analyzed in this study was a water-in-glass evacuated tube solar water heater (Fig. 2). This model was used to compare the performance of a 30 tube EVT system and a two panel flat plate collector. It was determined that the flat plate system had slightly higher energy savings when compared to the EVT system when operated in Sydney, Australia [16].
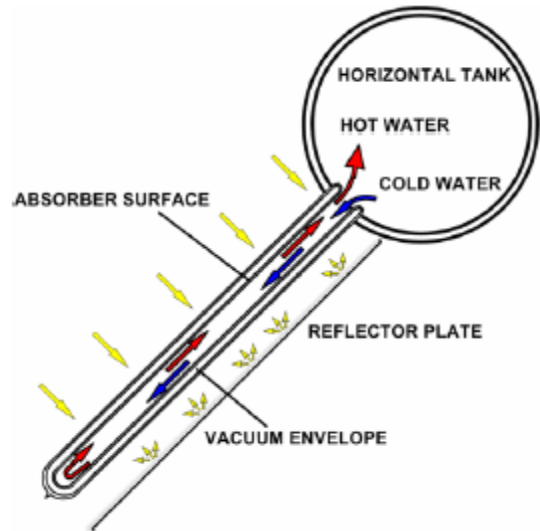
Figure 2. Water-in-glass solar water heater. Image Source [16]

Collector models can be used in a wide range of applications, and studies have utilized these models to predict the performance of EVT collectors with novel designs and configurations. A 2006 study conducted by Kim and Seo [17] revealed that the performance of EVT collectors varies with different shaped absorber tubes and varying configurations of the collector tubes. According to this study a U-tube welded onto a copper plate yielded the best results (Fig. 3) [17].
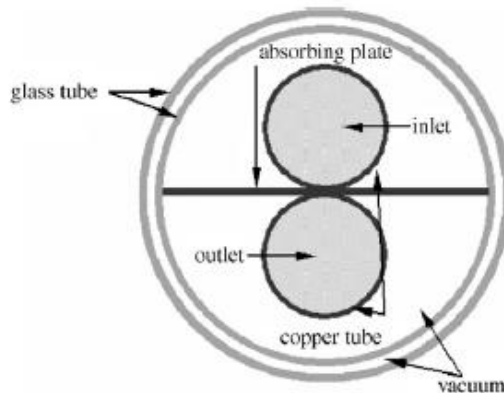
Figure 3. Cross-section of absorber tube design. Image Source [17]

Through a study completed by Sharma and Diaz [18], it was found that the performance of EVT collectors also improved when the absorber tube contains an array of minichannels. An interesting investigation into using supercritical carbon dioxide as the collector working fluid was performed by Zhang and Yamaguchi [19]. This study revealed an increase in collector performance with CO_2 as the working fluid when compared with water [19].

A similar analysis to the one presented in this document was performed by Ng et. al. in 2009 [20]. This analysis involved a thorough evaluation of the thermal losses throughout an evacuated tube heat pipe collector including the radiative heat loss between the absorber and ambient, radiative heat loss at the manifold, and the thermal resistance losses in the heat pipe and at the interface between the heat pipe condenser and manifold. The theoretical model was then validated against experimental data recorded for two different evacuated tube collectors: the Thermomax and BSERI collectors. Theoretical predictions of the useful heat gain were within 3-5% of the experimental results. [20]

A recent study was done analyzing the performance of a combined organic Rankine cycle (ORC) and vapor compression cycle refrigeration system. The ORC is a similar thermal engine to the DNEE in that both can operate on low grade heat [8]. Because of this, they can be very economical in smaller scale applications, and the heat source for these systems can come from a wide range of sources, including solar and waste heat utilization. Another advantage to this design is that current refrigeration systems can be retrofitted with compressors powered by these thermal engines with only slight modifications. The design of the combined ORC vapor compression cycle system can be seen in Fig. 4.

In this study, the combined system was designed with a 5 kW cooling

6

capacity and tested under laboratory conditions. After a thorough analysis the system was found to have achieved a 4.4 kW cooling output with a measured coefficient of performance of 0.48. These results prove that this combined system design can be very attractive when designed properly. [8]
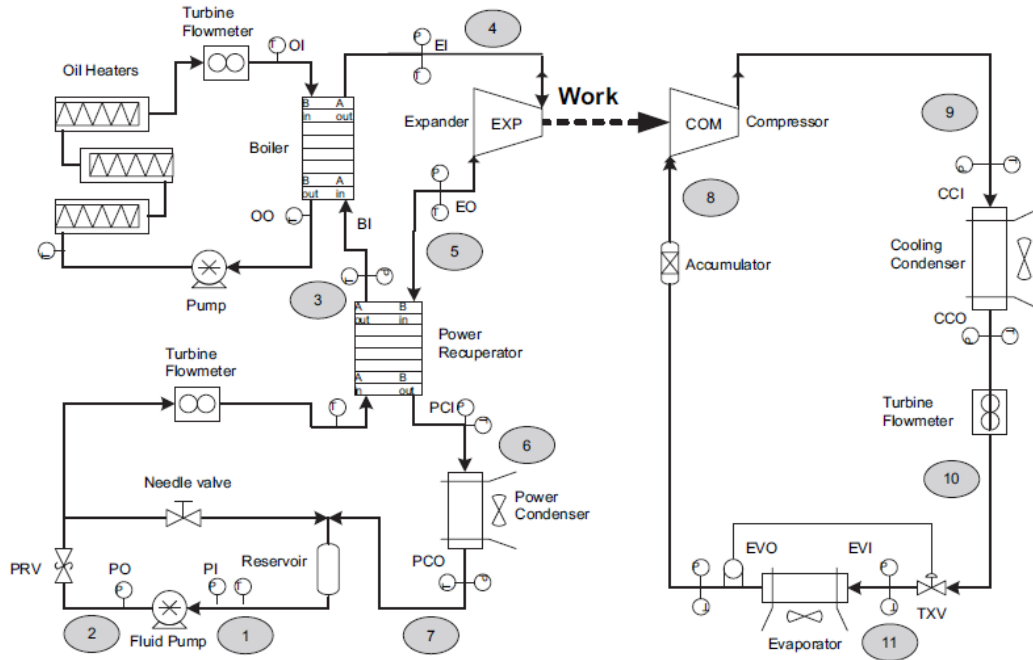
Figure 4. Combined ORC vapor compression system. Image Source [8]

CHAPTER 2

DELUGE NATURAL ENERGY ENGINE

2.1 - Overview

The Deluge Natural Energy Engine (DNEE) is a thermal hydraulic engine developed by Deluge Inc. that takes advantage of the thermal expansion properties of fluids to convert thermal energy to mechanical energy [4]. By simply adding and removing heat from the system, useful work can be generated to accomplish a wide range of tasks. Fig. 5 shows a picture of the DNEE associated with this project.

Figure 5. Deluge Natural Energy Engine

The DNEE consists of a simple design incorporating a piston-cylinder arrangement with a heat exchanger. The cylinder contains the piston and a working fluid, which is carbon dioxide. The engine cycles by adding and removing heat from this working fluid. In this case, water is used as the heat transfer fluid. When adding heat, the carbon dioxide thermally expands and pushes the piston out. Heat is then transferred out of the working fluid completing the cycle and returning the piston to its original position, see Fig. 6. [4]
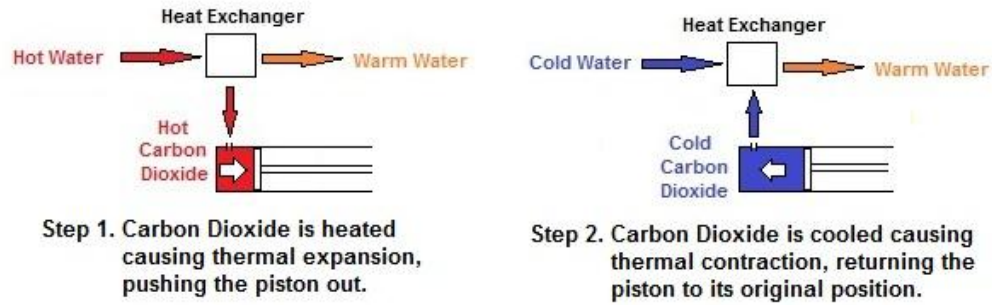
Figure 6. Operation of the DNEE

Possibly the most attractive attribute of this system is its ability to operate at surprisingly low temperatures. According to Deluge Inc., the DNEE is capable of operating at a hot supply temperature of only 82°C (180°F), with the heat dump at approximately 27°C (80˚F). Because of this low temperature requirement, the heat source can be supplied from a wide range of sources, including waste heat, geothermal, solar, or even a simple water heater. [4]

Although the low temperature requirements of the engine afford flexibility, it is at the expense of the Carnot efficiency. Using equation 1 described by Çengel [21],

$$\eta_c = 1 - \frac{T_L}{T_H} \qquad [1]$$

where η_c is the Carnot (ideal) efficiency, T_L the heat sink (low) temperature, and T_H the heat source (high) temperature, we see that the Carnot efficiency for this temperature range is 15.6%. Currently, high-temperature Stirling Engines can operate at actual efficiencies between 30% and 40%, but they require a heat source at temperatures between 650 - 800°C [22], which can greatly limit the available sources for thermal energy.

9

2.2 – Deluge Natural Energy Engine Working Fluid

A considerable amount of analysis and consideration has been applied to the optimization of the DNEE working fluid. Because the engine operates on the thermal expansion and contraction of the working fluid, it is very important to find a substance that expands substantially with a small amount of heat input. Ideally, the fluid would have a high coefficient of thermal expansion, β, with a low specific heat, c_p. This advantage can be seen by rearranging equation 2 from Çengel [21],

$$\Delta Q = m c_p \Delta T \qquad [2]$$

where ΔQ is the change in thermal energy, and m is the mass of the material being analyzed, solving for the change in the system's temperature, ΔT, and substituting into equation 3 from Çengel [23],

$$\Delta V = V_o \beta \Delta T \qquad [3]$$

yields,

$$\Delta V = \frac{V_o \beta \Delta Q}{m c_p} \qquad [4]$$

where ΔV is the change in the fluid's volume, and V_o is the initial volume of the fluid. Because the initial volume (V_o), mass (m), and thermal input (ΔQ), was held constant between the analysis of each fluid, the only terms that vary in this analysis are the coefficient of thermal expansion, β, and the specific heat, c_p, of each fluid. Therefore, to compare the suitability of each fluid for use in the DNEE, the ratio of the thermal expansion over the specific heat was used. This results in the equation,

$$X = \frac{\beta}{c_p} \qquad [5]$$

where X is called the thermal expansion ratio, which is used to compare the fluids.

Now each fluid can be analyzed and compared based on its inherent ability to accept a certain amount of heat energy and expand. This analysis was done for several fluids including carbon dioxide, water, R-134a, and many others. The fluids were each analyzed over the engine's typical operating range of temperatures and pressures using Engineering Equation Solver (EES) with built-in property functions [24]. Three-dimensional graphs were generated to find possible maximum and minima points over these temperatures and pressures and to more thoroughly analyze each fluid. It was found that of the fluids analyzed, the one with the best ratio of thermal expansion to specific heat was carbon dioxide. Figure 7 shows the three-dimensional plot for the thermal expansion ratio, X, for carbon dioxide.
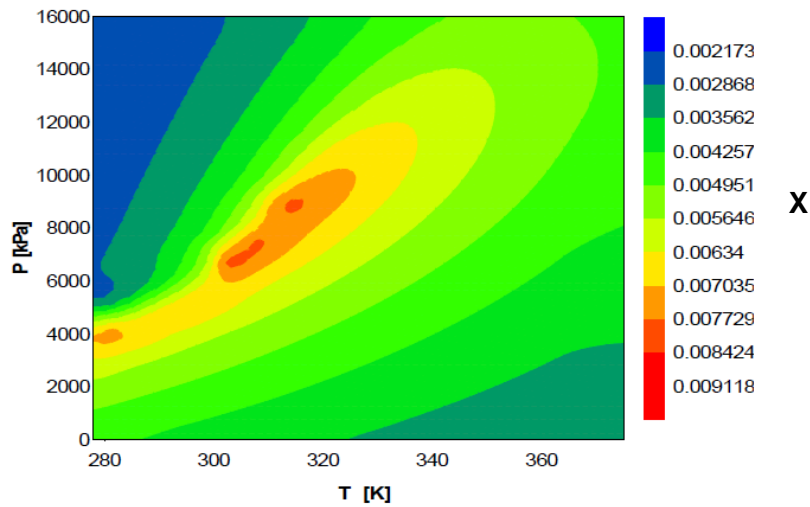
Figure 7. Thermal expansion ratio plot for CO_2

This result confirms previous analyses done by Deluge Inc. and supports their choice to use CO_2 as the working fluid for their engines. The remaining three-dimensional plots can be found in Appendix B.

2.3 – Original Design and Improvements to the DNEE

All of the original design and manufacturing work for the DNEE was done by Deluge Inc. This design, which can be seen in figure 8, consisted of two Deluge engines with the hot and cold water piping plumbed in parallel. Each engine contained its own piston cylinder, CO_2 heat exchanger, hot water pump, and cold water pump. All four pumps in the system were Grundfos UP26 99F 1/6 HP circulating pumps, see appendix C for the pump curve [25]. Both engines were plumbed together into one hot water loop and one cold water loop. The original heat source consisted of a single Rinnai R94LSe hot water heater capable of providing 199,000 Btu/hr [26], while the heat dump was an Amcot ST-40 cooling tower with a 480,000 Btu/h capacity [27] that removed thermal energy from the cold water loop through a plate and frame heat exchanger. The heat exchanger was a Tranter Inc. Superchanger plate and frame heat exchanger with a surface area of 17.43 ft^2 [28].
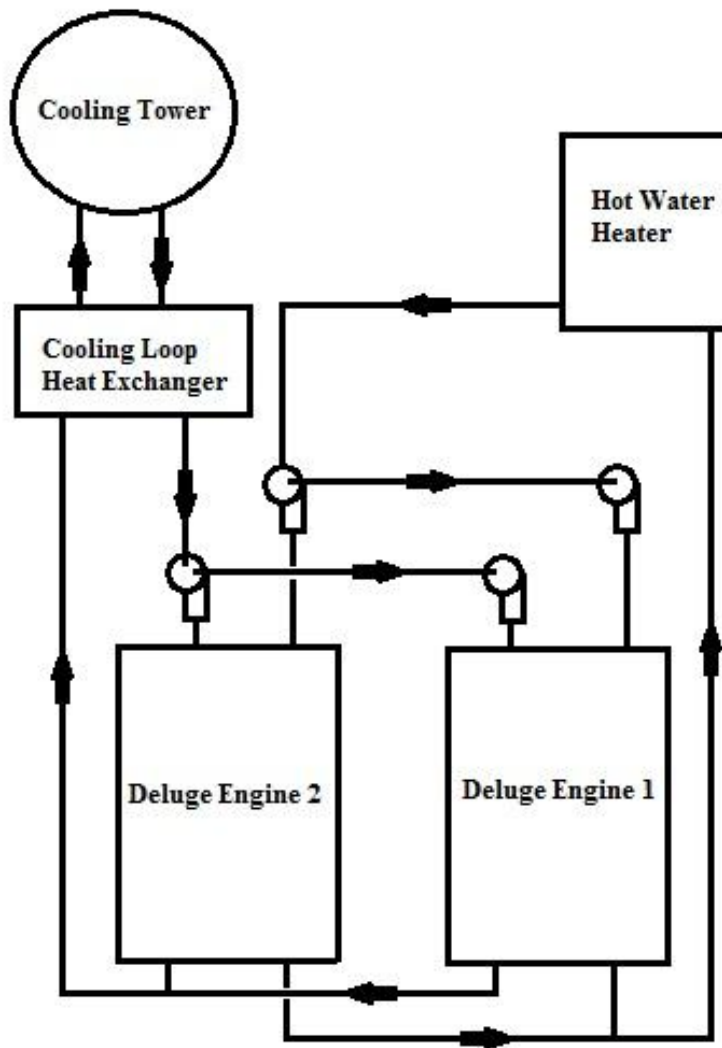
Figure 8. Layout of the Deluge Natural Energy Engine

The main heat source for the DNEE is the Rinnai R94LSe tankless instant water heater. A problem that was discovered with the tankless water heaters was their ability to regulate passing water flow. Based on several factors including incoming water temperature and the outlet temperature set point, the water heater uses a control valve to restrict the fluid flow in order to ensure an accurate outlet temperature [26], see Figure 9.

13
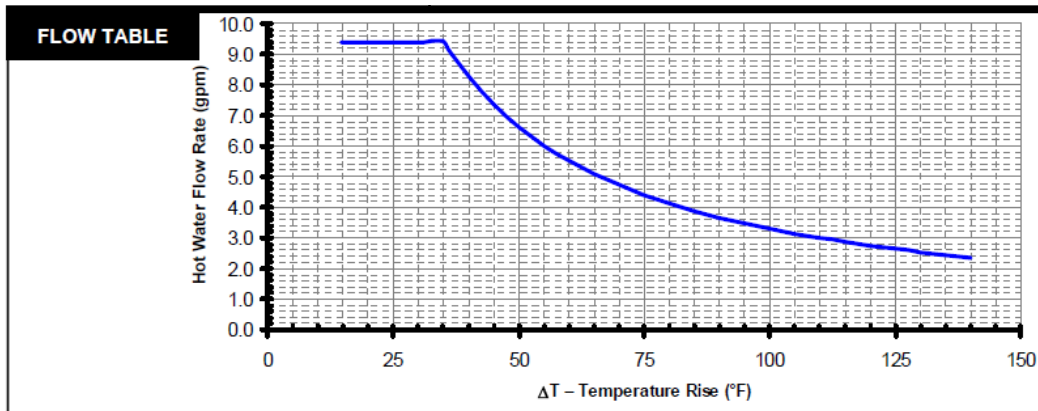
Figure 9. Designed water flow regulation by the Rinnai water heater. Image Source [26]

However, through testing it was found that the DNEE needed a much higher fluid flow to achieve the cycle speed needed for the full 10 tons of cooling. Therefore, the system has been redesigned to incorporate a second Rinnai water heater in parallel with the first heater, as seen in Figure 10. This significantly increased the flow rate of the hot water; however, this did not cause enough of a change to bring the engine to full functionality.

Figure 10. Rinnai Tankless water heaters plumbed in parallel

Along with the addition of the second hot water heater, larger water pumps were also installed on the system. Originally, 1/6 HP circulating pumps were installed on the hot and cold loops of both engines. In order to ensure the proper flow rates could be achieved, the four 1/6 HP pumps were replaced by two ½ HP Emerson C55 pumps, one on each the hot and cold loops, see Figure 11. However, even with major improvements to the water heating and pumping design, the system still did not perform at the level necessary for cooling extraction. Next steps to improve performance would be redesigning the heat exchanger on each engine in an attempt to improve the heat transfer efficiency. All efforts concerning the DNEE design and improvement, however, are out of the scope of this thesis.
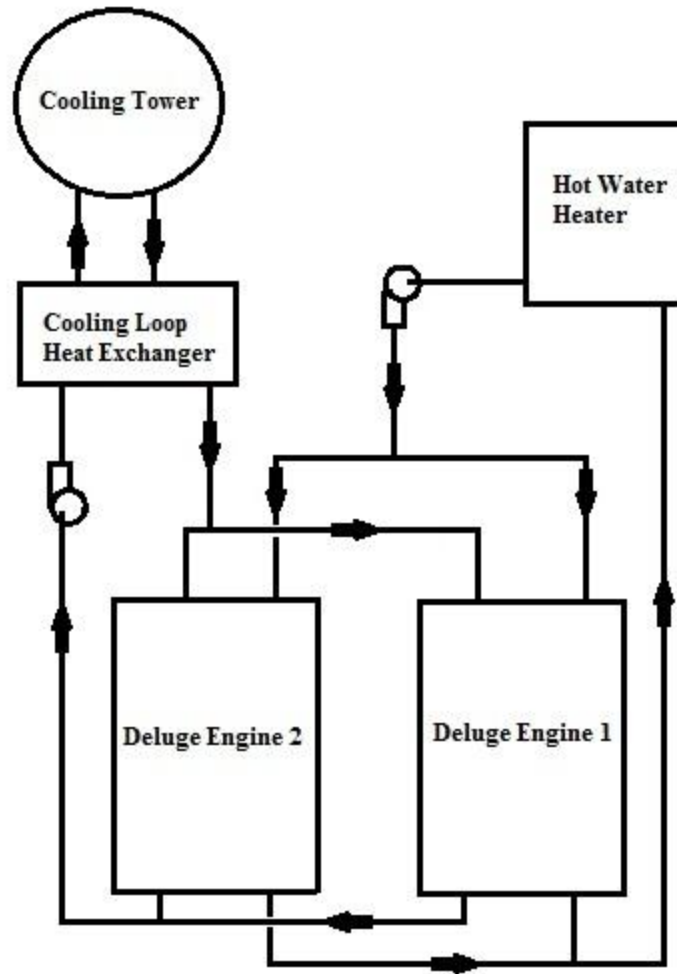
Figure 11. Deluge Engine with ½ HP pumps

2.4 – Integration of the DNEE into a Commercial Air Conditioning Unit

The ultimate goal of the Natural Energy Engine in this project is to completely replace the refrigerant compressor of a standard 10-ton air conditioning unit, essentially removing the largest load on grid power. This system has been targeted for primary use in commercial scale air conditioning and water chilling applications. A schematic showing the general operation of this system is shown in Figure 12.

16
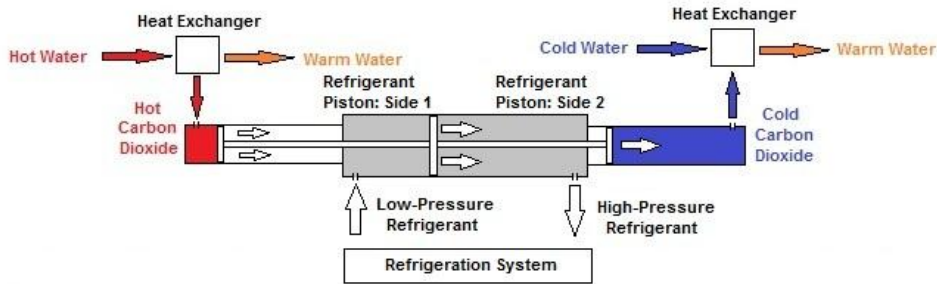
Step 1. Addition of heat in the left heat exchanger with heat removal in the right heat exchanger.
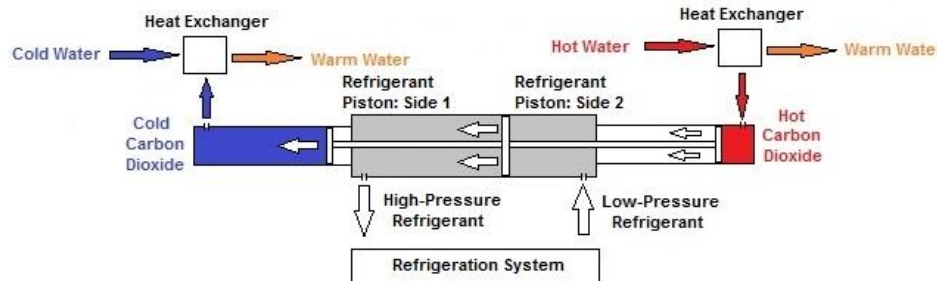
Step 2. Removal of heat from the left heat exchanger with heat addition to the right heat exchanger. System returns to original orientation.

Figure 12. Schematic of general operation of the DNEE refrigeration system

In the future, Deluge refrigeration systems would ideally be powered by solar thermal energy with a natural gas back-up. Unfortunately, for this analysis the solar array is only large enough to act as a pre-heater for the DNEE with the primary heat source coming from the Rinnai R94LSI natural gas instant hot water heaters.

Integration of the DNEE into the air conditioning unit was done using a relatively simple design. First, the original electric compressors were removed by cutting the drained refrigerant lines. New ¼" copper refrigerant lines were then run from the air conditioner to a flow control apparatus at each of the DNE engines. This flow control system uses check valves to direct the flow of refrigerant to and from the air conditioning system, see Figure 13. Once pressure

tested, the system was charged with R410-a by a trained air conditioning specialist.
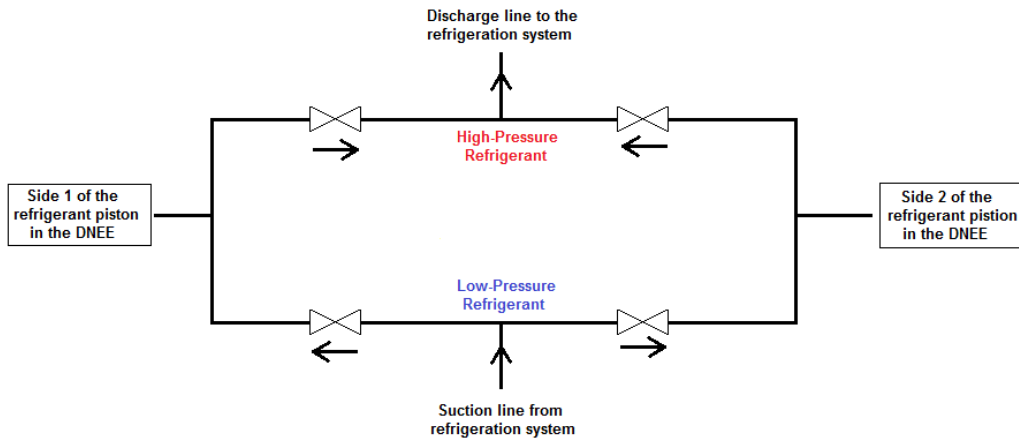
Figure 13. Diagram of the refrigerant flow control apparatus at the DNEE

CHAPTER 3

DESIGN OF THE SOLAR COLLECTOR EXPERIMENTS

3.1 – Layout and Setup of the Collector Array

When selecting a solar thermal collector it is important to note the cost and temperature requirements for the application. Some of the more prevalent collector designs include: flat plate, evacuated tube, parabolic trough, and parabolic dish collectors along with many other concentrating and non-concentrating designs [2]. In the case of this analysis, stationary evacuated tube collectors, which generate the necessary operating temperatures for most solar refrigeration applications, will be considered [5]. Because the addition of tracking systems increase the cost and complexity of a collector array, the use of a simple stationary evacuated tube array can save considerable amounts of money over the more complex concentrating and tracking collectors [5]. This makes them a very favorable option in solar refrigeration applications. When designing the layout of a solar collector array there are multiple factors that need to be considered for a successful system. This section will discuss these factors along with the reasoning behind each design decision.

According to the manufacturer, Apricus Inc., the collectors must be installed in groups of no more than 150 tubes in series. This is to prevent the possibility of boiling the water in the system. Therefore, when these collectors are used in larger scale applications, the Apricus AP-30 collectors are laid out in parallel rows of 150 tubes in series. Because the AP-30 collector contains 30 tubes, the max number of collectors per row is limited to five. [29]

Figure 14. Apricus AP-30 collector array

Using the model developed for the AP-30 collector, it was determined that the projected number of collectors required to operate the Deluge Engine solely on solar power exceeded the number of collectors available for the project. Therefore, all fifteen of the available collectors were installed and monitored for this project, seen in Figure 14. Following the guideline that no more than five collectors can be placed in series, the array was setup as a system of three parallel rows of five collectors in series. Figure 15 shows a schematic of the layout of the collector array.
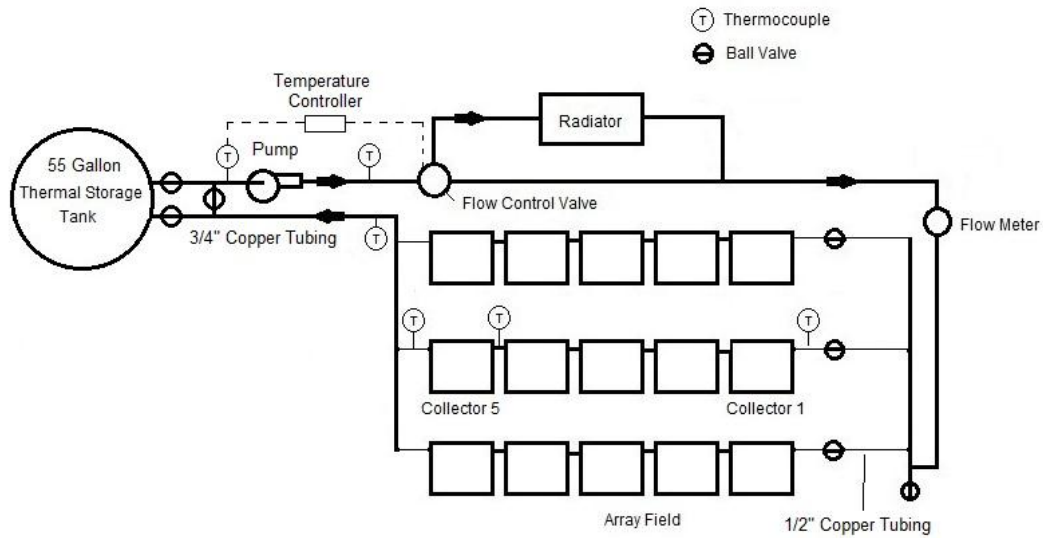
Figure 15. Layout schematic of the solar array

To give the user the ability to turn on and off each row, ball valves were installed at the inlet of each of the three rows. The ¾" copper water lines running from the thermal storage tank to the collector array were designed to have equal head loss in each of the three collector rows. This was achieved by setting the inlet and outlet of the water lines at the collectors on opposite corners of the array, see figure 15. The thermal storage tank consisted of a metal 55 gallon drum that had been adapted to include threaded ports for easy installation of the plumbing lines. Figure 16 shows a picture of the storage container, heat dump, and control valve.

Figure 16. Storage tank, heat dump, and flow control valve

In an effort to save money, one of the Grundfos UP26 99F 1/6 HP pumps removed from the Deluge Engine was reused as the solar array circulating pump because of its appropriate size and availability. The flow rate in this system is monitored with an inline turbine flow meter. Table 1 gives an overview of the instruments used to monitor the collector array.

Table 1. Collector Array Instruments

Instrument	Manufacturer	Model Number	Measurement Range
Flow Meter	Onicon Inc	F-1310	0-25 GPM [30]
Thermocouples	Omega	SA1-T	-60°C - 175°C [31]
Thermocouple Extension Wire	Omega	EXTT-T	N/A [31]
Data Acquisition	National Instruments	NI DAQ 9174	N/A [32]

When using a solar thermal array to power this system it is important to protect the collectors from overheating. The collectors could easily be covered to protect them from overheating when in danger; however, an automated design would be more favorable since an operator may not be on site at all times. This

process can be done automatically many different ways with cost and reliability being heavily considered in the design. A simple and cheap solution to protect the collectors from overheating would be to incorporate a prismatic structure to the collector design [33]. Based on the collector temperature, this prismatic structure regulates the amount of light reaching the absorber [33]. Another simple solution would be to constantly run the circulating pump during the daylight hours and heavily rely on a heat dump to remove excess heat from the system to maintain the collector temperature. Because of the high likelihood of the working fluid boiling when no load is present, it was determined that a heat dump was needed for the system. The heat dump selected for this array was a car radiator and fan assembly installed in parallel to the main line. A Bi-Torq flow control valve that operates on a 24V power source was also installed to direct the flow through either the main line or the heat dump depending on the temperature of the fluid coming from the storage container. A picture of the heat dump can be seen in Figure 17. An overview of the equipment used in this system is shown in table 2.

Figure 17. Heat dump for the collector array

Table 2. Equipment List

Equipment	Manufacturer	Model Number
Control Valve	Bi-Torq Valve Automation	1S3WT15400E34 [34]
Radiator	Spectra Premium	CU1830 [35]
Pump	Grundfos Pumps Corporation	UP26 99F [25]
Pump Timer	Intermatic, Inc.	T101R [36]
12VDC Supply	Astrodyne	SP-240-12 [37]
24VDC Supply	Astrodyne	SP-320-27[37]
Relays	Omega	SSRDC100VDC20 [31]
Heat Dump Fan	TorqFlo	733700 [38]

Temperature was monitored throughout the collector array. Type-T thermocouples were placed at the inlet and exit of the thermal storage container as well as at three different points in the array's middle row, which included the inlet, in between the fourth and fifth collectors, and the outlet. These points were selected to give an in-depth view of the performance of both a full row of collectors, as well as that of a single collector.

3.2 – Collector Tilt Optimization

To optimize the performance of a solar array, it is important to determine the optimal tilt angle for the collectors. Furthermore, it is important to optimize the tilt angle for the time of the year when the solar energy is needed most. In the case of this system, where the resulting hot water is used to supply thermal energy to power a refrigeration system, the emphasis on performance should be placed on the summer months. Therefore, an analysis was done using the model developed for the Apricus AP-30 collectors to optimize the tilt angle of the collectors during the summer. For this analysis, the summer months were considered to be from May to October. This was decided upon by referencing the Salt River Project Utilities (SRP) website. Under the SRP time-of-use energy rate plan, the summer billing months are listed from May to October and, therefore,

was determined to be a good approximation of the peak air conditioning months for Phoenix, AZ [39].

According to Apricus, optimal heat pipe performance is achieved between a tilt angle of 20° - 70° [29]. Therefore, the absorbed solar radiation by the collectors was analyzed in tilt angle increments of 5° over the recommended tilt angle range. The analysis was done from 8 AM to 4 PM to ensure that the sun was up during the time period over the course of the entire year. The total absorbed solar radiation for an entire year as well as the summer months was then calculated for each angle.
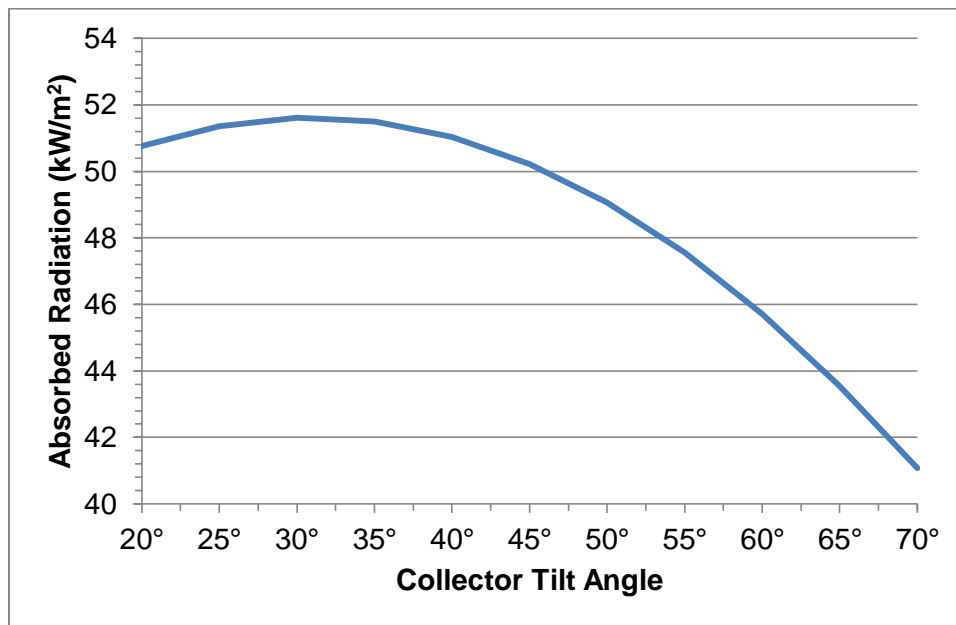
Figure 18. Total absorbed solar radiation for the entire year

Figure 18 shows the projected total absorbed radiation over an entire year for each angle analyzed. In this analysis, the maximum absorbed solar radiation occurs around a tilt angle of 30°. Although analyzing the system over

the entire year gave deeper insight into the annual performance, more weight

should be placed on the performance of the collectors during the summer
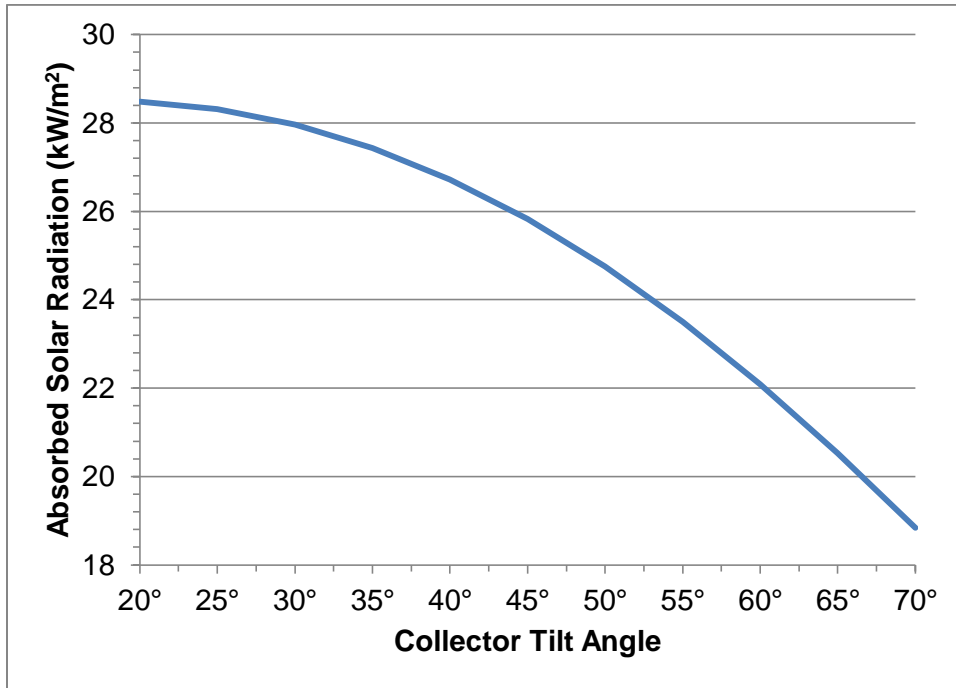
months.

Figure 19. Total absorbed solar radiation for May to October

Figure 19 shows the total absorbed solar radiation over the summer

months of May to October. While the analysis of the entire year showed that a tilt

angle of approximately 30° would be best; when focusing on the summer

months, it becomes clear that the minimum tilt angle of 20° is most beneficial

during the crucial time from May to October.

Table 3 shows the absorbed solar radiation at each angle on a summer

and annual basis. These are the same results represented in figures 18 and 19.

The "compared to max" calculation in the table represents the decrease in

absorbed solar radiation for each angle setting when compared to the optimal tilt angle for the summer and annual analysis. When looking at the data in table 3, it was noted that by increasing the tilt angle from 20° to 25° the annual absorbed solar radiation increased by nearly 600 W/m^2 with only a drop of 160 W/m^2 during the summer months. This was determined to be a fair tradeoff and led to the selection of 25° as the collector tilt angle for this array.

Table 3. Total annual and summer absorbed solar radiation

Tilt Angle	Summer [W/m^2]	Compared to Max [W/m^2]	Annual [W/m^2]	Compared to Max [W/m^2]
20°	28476	0	50764	-842
25°	28316	-161	51363	-243
30°	27967	-509	51606	0
35°	27431	-1045	51497	-109
40°	26715	-1761	51036	-571
45°	25821	-2655	50225	-1382
50°	24749	-3727	49062	-2544
55°	23504	-4972	47556	-4051
60°	22091	-6385	45708	-5899
65°	20528	-7949	43539	-8067
70°	18839	-9637	41077	-10529

3.3 – Control System for the Collector Array

A control system was incorporated into the collector array to optimize the performance of the system without constant monitoring and adjusting from the user. The main points of control in the collector array were turning the system on and off along with controlling the direction of the fluid flow between the main line and the heat dump. Cost and simplicity were the two main factors governing the design of the control system.

Controlling the power supply to the system was achieved through using an Intermatic T101R pool pump timer, which is capable of handling 40 Amps of

current. It was important to completely shut down the fluid flow in the system in the evening in order to maintain the temperature in the thermal storage container overnight. If the system was allowed to run throughout the night, the fluid would be exposed to the heat losses in the entire system as opposed to just the losses in the storage container. This would lead to increased heat loss overnight which decreases the effectiveness of the thermal storage. The pool pump timer was used to control the power being supplied to both the circulating pump and the heat dump fan. Therefore, in the morning, when the timer was set to turn on, both the pump and fan were started. To ensure that no solar energy was wasted and that the water in the system was not boiled off, the pump was set to turn on at 5:00 AM and turn off at 8:00 PM. This ensured that the pump would be running the entire time the sun was up every day of the year. To optimize the operation for a particular time of year, the timer could easily be adjusted to match the sunrise and sunset times for that time of year.

The other important point of control in the system was manipulating the direction of the fluid flow between the main line and the heat dump. This was achieved by using a simple temperature PID controller from Omega Engineering. The Omega CNi3244 controller received temperature information from a T-type thermocouple placed at the exit of the thermal storage container. Once this temperature reading reached 80°C, the controller used a DC pulse to activate a relay that sent the required 24V power supply to the control valve, changing the direction of the flow toward the heat dump. Once the temperature of the fluid at the outlet of the thermal storage dropped below the 80°C threshold, the controller sent a DC pulse to a second relay opening the circuit to the control valve diverting the flow back to the main line. The 80°C threshold was determined by

28

analyzing the temperature increase of the working fluid using the model designed

for this collector array. The peak temperature gain according to the model occurs

at 1 PM during the month of June, therefore, this was the time selected for this

analysis. In this analysis the flow rate was set to 4 GPM, slightly lower than the

capability of the pump, to ensure a built-in buffer to accommodate a potential

drop in the flow rate. Once these parameters were entered into the model, it

projected a temperature rise of 13.8°C. This placed the fluid exit temperature

safely under the boiling point at 93.8°C. This design allowed the system to build

and maintain high temperatures with a thermal load while also allowing for

thermal energy to be dumped when the fluid temperature becomes too high.

Figure 20 shows a picture of the flow control system used for this array.

Figure 20. Collector array fluid controller

3.4 – Summary

The layout of the array of Apricus AP-30 collectors was designed based on manufacturer recommendations as well as calculations using the model designed for these collectors. The manufacturer recommended that the collectors be installed in banks of no more than 150 tubes in series. For the AP-30 collector, which contains 30 tubes in series, this means that each row can consist of no more than five collectors in series. Therefore, the array was designed and constructed as three parallel rows of five collectors in series totaling fifteen Apricus AP-30 collectors. To equalize the fluid flow rate in each row, the plumbing was designed with the fluid inlet and outlet located in opposite corners of the array. This ensured equal head loss in each row and by extension an equal flow rate. An analysis was also done to determine the optimal tilt angle for the collectors. By using the model developed for the Apricus AP-30 collectors, the best tilt angle for this system was determined to be approximately 25°.

CHAPTER 4

APRICUS AP-30 COLLECTOR MODEL

4.1 – Overview

The updated collector model discussed in this analysis is a modified
version of the Microsoft Excel computer model created by Witt [3]. Any further
detail on the design and programming of the original Witt model not covered in
this document may be found in [3].

The original Witt Model was designed to predict collector performance for
the Apricus AP-30 system given varying environmental conditions. This was
achieved through calculating the useful gain from the collector array along with
the temperature gain of the heat transfer fluid in thermal storage. Additional
modifications have been made to this model to more accurately predict the useful
gain. By incorporating the temperature rise of the heat transfer fluid through the
collector array and correcting some minor errors present in the original model a
more accurate prediction of the collector performance can be made. The revised
model also predicts the temperature rise of the heat transfer fluid across each
collector in the series of five. It should also be noted that the Updated Witt model
remained as a Microsoft Excel spreadsheet.

4.2 – Witt Model

The Witt model included an in-depth calculation of the absorbed solar
radiation of the collectors. This involved calculating the beam, diffuse, and
ground reflectance components of solar radiation using methods discussed by

Duffie and Beckman [7]. When all of these factors are combined they result in the absorbed solar radiation, S,

$$S = I_b R_b (\tau\alpha)_b + I_d (\tau\alpha)_d \left(\frac{1 + cos\theta}{2}\right) + \rho_{gr} I (\tau\alpha)_{gr} \left(\frac{1 - cos\theta}{2}\right) \qquad [6]$$

where θ is the collector tilt angle, ρ_{gr} is the ground reflectance, and the subscripts b, d, and gr represent the beam, diffuse, and ground reflectance components of the solar radiation, respectively. The total solar insolation value, I, for this model was obtained using AZMET data from the Phoenix Encanto Weather Station in Phoenix, AZ [40]. Using equations from Duffie and Beckman [7], the beam fraction, I_b, and diffuse fraction, I_d, were calculated. Because the beam and diffuse fractions can vary widely depending on environmental conditions the hourly clearness index, k_T, was incorporated to account for these variations. The hourly clearness index is defined as the ratio of total solar insolation on a horizontal surface, I, to the extraterrestrial solar insolation, I_o. Because the total solar insolation data listed by AZMET is for a horizontal surface, the ratio of beam radiation on a tilted surface to the beam radiation on a horizontal surface, R_b, is used to accurately determine the actual beam radiation on an angled collector. The transmittance-absorptance product, $\tau\alpha$, was also factored into the model to represent the properties of the cover and absorber materials. An in-depth analysis of the transmittance and reflectance losses of the cover was done to determine the actual incident radiation on the absorber surface. [3]

The model designed by Witt also included the inefficiencies associated within the solar collector. This included the thermal energy losses at the absorber as well as at the manifold. Other losses in the solar collector included the heat pipe conduction and convection thermal resistances at the condenser and

working fluid interface, which were calculated by using the methods described in

[20]. A diagram of the thermal resistance network can be seen in figure 21.
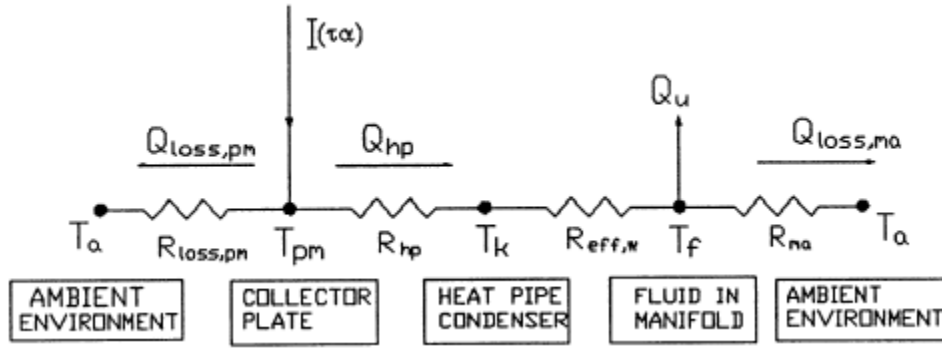
Figure 21. Thermal resistances of an EVT heat pipe collector, Image source [20]

Once all of the thermal losses were factored in, the collector efficiency

factor F was calculated using

$$F' = \frac{1}{1 + \frac{R_{hp}}{R_{rad}} + \frac{R_{eff,w}}{R_{rad}}}$$

[7]

[3, 20]. Physically, the collector efficiency factor represents the ratio of actual

useful energy gain to the useful energy gain that would be experienced if the

collector's absorber was at the fluid temperature [7]. From the calculated value of

F the collector heat removal factor, F_R, can be calculated using,

$$\frac{F_R}{F'} = \frac{\dot{m}c_p}{A_c U_L F'}\left[1 - e^{-\frac{A_c U_L F'}{\dot{m}c_p}}\right]$$

[8]

where A_c is the collector surface area, U_L is the overall collector heat loss, $\dot{m}$ is

the mass flow rate of the heat transfer fluid, and c_p is the specific heat of the

transfer fluid [3, 7]. The useful heat gain, Q_u, was then calculated using,

$$Q_u = A_c F_R[S - U_L(T_i - T_a)]$$

[9]

where T_i is the inlet temperature, and T_a is the ambient temperature [3, 7]. Duffie and Beckman [7] note that the heat removal factor and useful heat gain equations, Eq. 8 and 9, developed for plate and tube solar collectors can also be applied to most other collector designs, which was assumed to include the evacuated tube-heat pipe design utilized in the AP-30 collector.

One goal of this model is to predict the temperature rise of the heat transfer fluid in the storage container of the collector array for a given period of time. This is done by setting up an energy balance on the storage reservoir and using the useful heat gain over a set time period as the thermal input. The equations defining the energy balance at the thermal reservoir will be discussed in further detail in section 4.3.

4.3 – Model Modifications

During an in-depth analysis of the Witt Model, it was determined that several adjustments needed to be made to more accurately reflect its capability. This led to a re-design of the model, resulting in a simpler user interface along with corrections to calculation errors originally present. A comparison between the results of the Updated Witt model, the original Witt model, and the SRCC efficiency curve will be done to determine the accuracy of each method.

The changes to the Witt model included one major correction to the calculation of the heat transfer surface area between the heat pipe and the working fluid. In the Witt model this area was mistakenly calculated using the formula for the volume of a cylinder. This resulted in a calculated thermal contact area much smaller than the true value. The miscalculated contact area had a major impact on the thermal transfer between the heat pipe and working fluid,

34

which ultimately impacted the collector efficiency factor, collector loss coefficient, and the overall accuracy of the model. Once corrected, the calculated surface area changed from 0.000011 m^2 to 0.0022 m^2, which was a significant adjustment. This resulted in an increase in the collector efficiency factor and a decrease in the collector loss coefficient. This would be expected since more thermal energy can be transferred to the working fluid as opposed to being lost to the surroundings.

In an attempt to minimize the error from using environmental data from previous years, a four-year average of the AZMET data replaced the single year data used by the Witt model. The Updated Witt model now uses the average monthly data over the years 2007, 2008, 2009, and 2010. Because these years were so recent, it was determined that they would be the best representation of the current year. Previously, the Witt model only used environmental data recorded in 2007. Moving to the four-year average was a good step toward minimizing the impact of environmental variability from year to year. The Updated model was also adapted to include environmental data for the entire year, while the Witt model originally contained only data from April to September.

Originally, the Witt Model was designed to predict the output of a single row of collectors. However, in many applications the solar array must be setup as multiple rows of collectors in parallel. By doing this, the flow is split, and the rate seen by each row is reduced impacting both the heat transfer capabilities and temperature rise of the working fluid. To easily account for the multiple rows, a user input was incorporated into the program allowing for the number of collector rows to be introduced into the calculation. It was assumed that the flow through each of the rows was equal. Therefore, the total flow rate is divided by the

35

number of collector rows resulting in a flow rate per row, which is then used to calculate the heat transfer coefficient and the temperature rise of the working fluid.

In the Witt Model, the heat loss experienced at each tube was assumed to be equal to the loss experienced at the first tube. This method does not include the increased thermal loss as the temperature of the heat transfer fluid rises through the system. To account for this, the model was adapted to calculate the temperature rise of the fluid across each tube using equation 9 along with equation 10:

$$T_o = T_i + \frac{Q_u}{\dot{m}c_p}$$
[10]

where T_o is the temperature at the outlet of each tube. It was then assumed that the outlet temperature from one collector tube was the inlet temperature of the next tube. Once this was determined, the useful heat gain from each tube could be determined by analyzing one tube at a time in a step-wise method through the entire collector row. Therefore, the outlet temperature of the complete collector array is the temperature of the working fluid at the exit of the final tube in a row. This can be assumed because the system was designed to have equal flow through each row and each collector should be receiving the same amount of solar radiation.

An alternate way to account for the decreasing efficiency through the array is shown in equations 11 and 12. It has been shown that for N identical collectors in series, the overall heat removal factor can be expressed as [7]

$$F_R U_L = F_{R1} U_{L1} \left(\frac{1 - (1 - K)^N}{NK} \right)$$
[11]

where

$$K = \frac{A_N F_{RN} U_{LN}}{\dot{m} c_p} \qquad [12]$$

The heat removal factor calculated in equation 11 takes into account the decreased collector efficiency experienced as the fluid temperature increases through the array. Therefore, this overall F_R can be used to account for the decreasing efficiency instead of using the iterative calculation described above.

The method behind calculating the thermal storage temperature after a given period of time was also altered in the updated model. In the Witt Model this temperature was calculated with the assumption that the fluid temperature in the storage tank and at the inlet of the collector array was constant over the period of the analysis. However, in practice, the temperature of the fluid is constantly increasing during the day resulting in changes to the heat loss in both the collectors and the storage container. Therefore, a custom Excel macro was developed to constantly update the temperature of the fluid in the storage container, which then becomes the fluid temperature at the inlet of the array. The analysis is done in one second steps up to the time length that the user dictates at the beginning of the Excel macro. Therefore, in equation 13 the value of the change in time, Δt, is equal to one throughout the iterative calculation:

$$T_s = T_{i,s} + \frac{\Delta t}{(m c_p)_s}[Q_u - L_s - (UA)_s(T_s - T_a)] \qquad [13]$$

In equation 11 T_s is the temperature of the storage container after some time t, $T_{i,s}$ is the initial temperature of the storage container at the start of the time step, $(mc_p)_s$ is the mass-specific heat product of the fluid in the storage container, L_s is the thermal load on the storage container, and $(UA)_s$ is the storage loss coefficient-area product.

In an attempt to simplify the operation of the model, a control panel was added, which includes inputs for all of the user controlled values, see figure 22. These inputs feed into the model, and the fluid exit temperatures for both the updated model and the SRCC curve are calculated and displayed on the control panel. Also displayed on the control panel is the efficiency of the updated model and the SRCC curve along with the temperature of the working fluid between the fourth and fifth collectors in a row. The temperature between the fourth and fifth collectors was calculated to compare with the thermocouple reading at the same point on the actual array. This thermocouple was installed as a way to monitor the performance of a single collector.

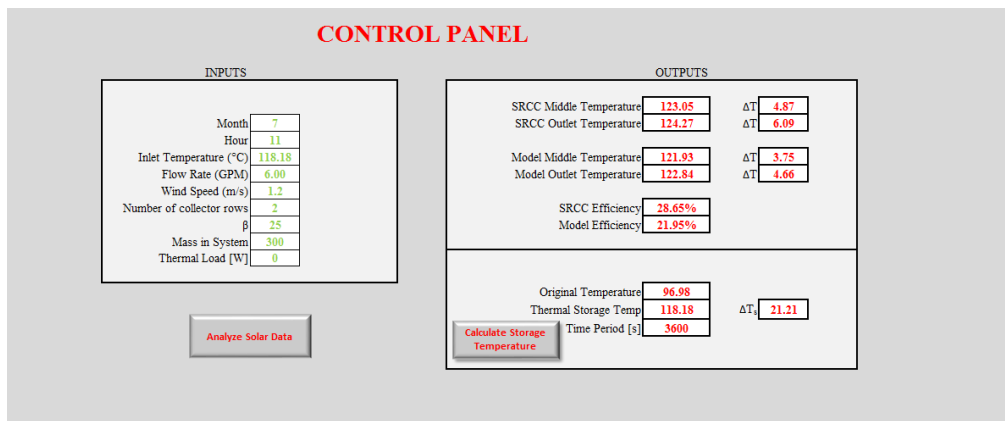

Figure 22. Control panel of the updated model

Since the two models and the SRCC efficiency curve will be compared by their ability to predict the outlet temperature of the collector array, a calculation was designed to compute the predicted outlet temperature using the SRCC efficiency curve. The SRCC predicted efficiency, η_{SRCC}, was first used to calculate the useful heat gain Q_u:

$$Q_u = \eta_{SRCC} I A_c \qquad\qquad [14]$$

This calculated useful absorbed energy was then used to compute the temperature rise of the fluid and the outlet temperature of the collector array using equation 10 discussed above.

Finally, to introduce the ability for bulk analysis of data, multiple excel macros were written to automatically calculate predicted temperature values in all three models. Recorded fluid flow rate, month of the test, hour of the test, and fluid inlet temperature for the entire test period is entered into the data analysis sheet. Once the data sheet is complete, the user clicks the "analyze solar data" button on the control panel to run the macro that calculates the temperature values in the system for all time points entered. This allows for easy analysis of a full day of data.

4.4 – Summary

Major adjustments were made to the operation of the Witt model. A large correction to the calculation of the heat transfer area between the heat pipe and the fluid ultimately led to an increase in the predicted system efficiency determined by the model. The Witt model was also changed from using a single year of environmental data for predictions to a four year average. Adjustments were also made to the calculation of the thermal storage temperature and the thermal loss in the array. The user interface of the program was simplified for ease of use and macros were programmed into the models to analyze data in bulk.

CHAPTER 5

MODEL VALIDATION AND DISCUSSION

5.1 – Overview

Both the Witt model and the updated model for the Apricus AP-30

collectors were developed using an in-depth analysis of all system losses. The

calculations in these models were also extensively reviewed prior to use.

However, to ensure the accuracy of both models, a thorough investigation was

done comparing the expected collector output from the models to the actual data

collected for the Apricus collector array described earlier in this document. Data

was collected during the months of June, July, and August 2011. The collector

array was built and tested on the rooftop of the Engineering Building F-Wing at

Arizona State University in Tempe, AZ.

In this investigation a comparison was done on the accuracy of the Witt

Model, SRCC efficiency curve, and the Updated Witt Model. In order to remove

the error present from using environmental data from previous years, the models

were adapted to receive the actual recorded environmental data for the test

periods. By doing this, a more accurate analysis of the error in each model can

be performed. The related environmental data for every test was taken from the

AZMET website [40] and introduced into the model. The models were then

compared based on the percent error of their temperature calculations for the

system.

As previously explained, the solar array was designed as three rows of

five collectors in series. During an initial test of this design, it was determined that

the heat dump built for the system was too small to handle the amount of thermal

energy that needed to be removed from the fluid with all three collector rows active and no load placed on the system. Therefore, during the multiple row tests only two of the three rows were active. For this analysis it was assumed that the method used for scaling the model up to two rows can also be applied to systems larger than two rows. While the bulk of the investigation was done on analyzing two active collector rows, an initial analysis was done on a single row of collectors.

5.2 – Error Analysis

To represent the various uncertainties in the study, an error analysis was done. The errors incorporated into the analysis were the measurement uncertainties of the fluid flow meter, thermocouples, and data acquisition system as well as the errors in recording the environmental data by AZMET. A summary of these errors can be seen in table 4.

Table 4. Summary of Measurement Errors

Equipment	Error
National Instruments NI9213 thermocouple module	2.6°C [41]
Omega T Type Thermocouple	1°C [42]
Onicon 1310 Flow Meter	0.5% [30]
National Instruments NI9205 Voltage module	0.006V [43]
AZMET Air Temperature	0.4°C [40]
AZMET Solar Radiation	5% [40]

Because measured quantities were being introduced into the models, primarily in the useful heat gain equation, propagation of the errors through each calculation was done, and the overall error of each model was determined for the validation process. For addition and subtraction steps, equation 15 was used to determine the error of the calculated value, while equation 16 was used for multiplication and division steps [44].

$$\delta q = \sqrt{\delta x^2 + \cdots + \delta z^2} \qquad\qquad [15]$$

$$\frac{\delta q}{|q|} = \sqrt{\left(\frac{\delta x}{|x|}\right)^2 + \cdots + \left(\frac{\delta z}{|z|}\right)^2} \qquad\qquad [16]$$

In equations 15 and 16, δq is the uncertainty in the calculated value q, where x and z are values that comprise the calculation of q, and δx and δz are the uncertainty in x and z, respectively.

5.3 – Single Collector Row Validation

Testing on a single row of Apricus AP-30 collectors was performed on June 29th and June 30th 2011. Partial shading of the array occurred early in the morning as well as later in the afternoon. Therefore, data was recorded between the hours of 10AM and 3PM for the single row experiments. This was to ensure that the entire collector array was receiving full sunlight throughout the entire test.

The single row analysis was done as an initial test of the data acquisition system and the accuracy of the models. Fluid flow was valved off for the first and last row of the array. This diverted all flow through the middle row, which was being monitored for temperature at the inlet, before the last collector, and the outlet of the row. This data was then compared to the predictions of the three models. Figure 23 shows the recorded and calculated outlet temperatures for the experiment performed on June 29th.
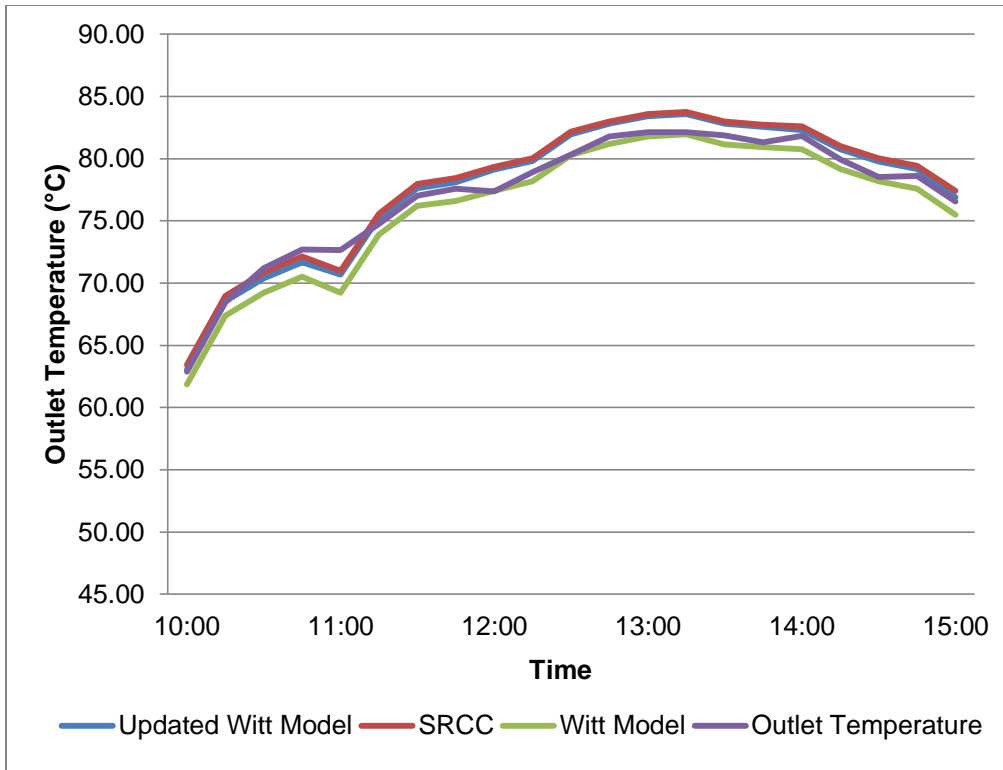
Figure 23. Outlet temperatures for June 29th

The same analysis was repeated for the data recorded on June 30th, and the outlet temperatures are shown in figure 24.
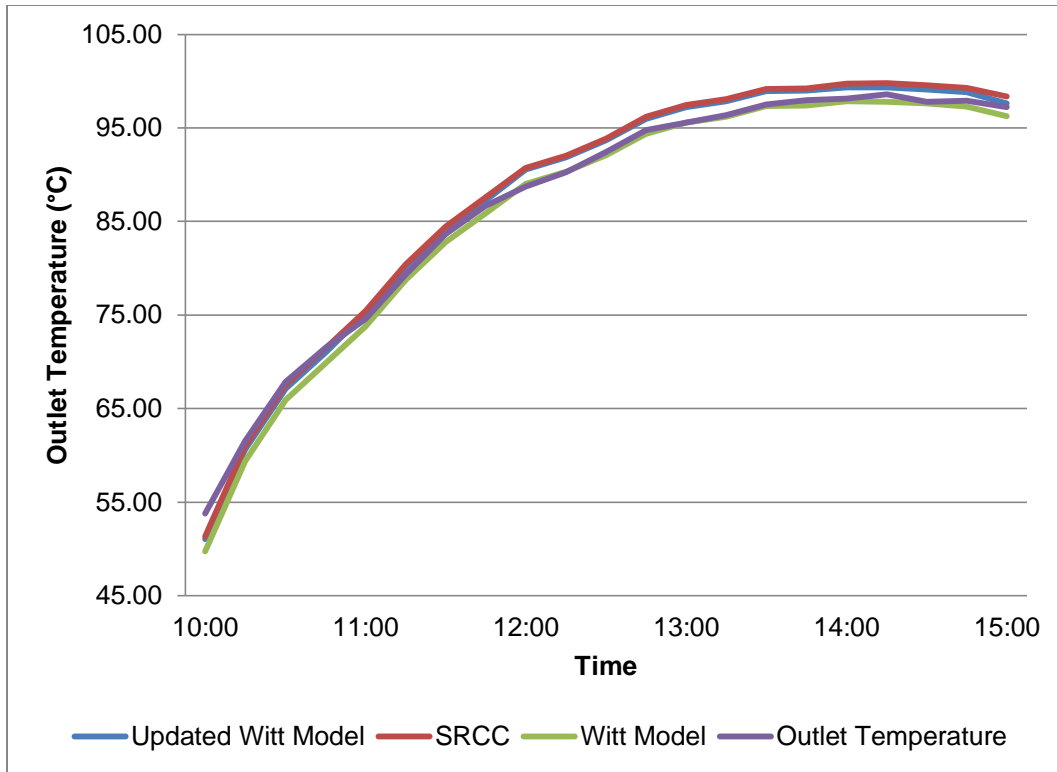
Figure 24. Outlet temperatures for June 30th

To give a direct comparison of each model, the percent error was determined for the values calculated by each model. Figure 25 shows the average percent error for the two models and the SRCC curve over the two day test.
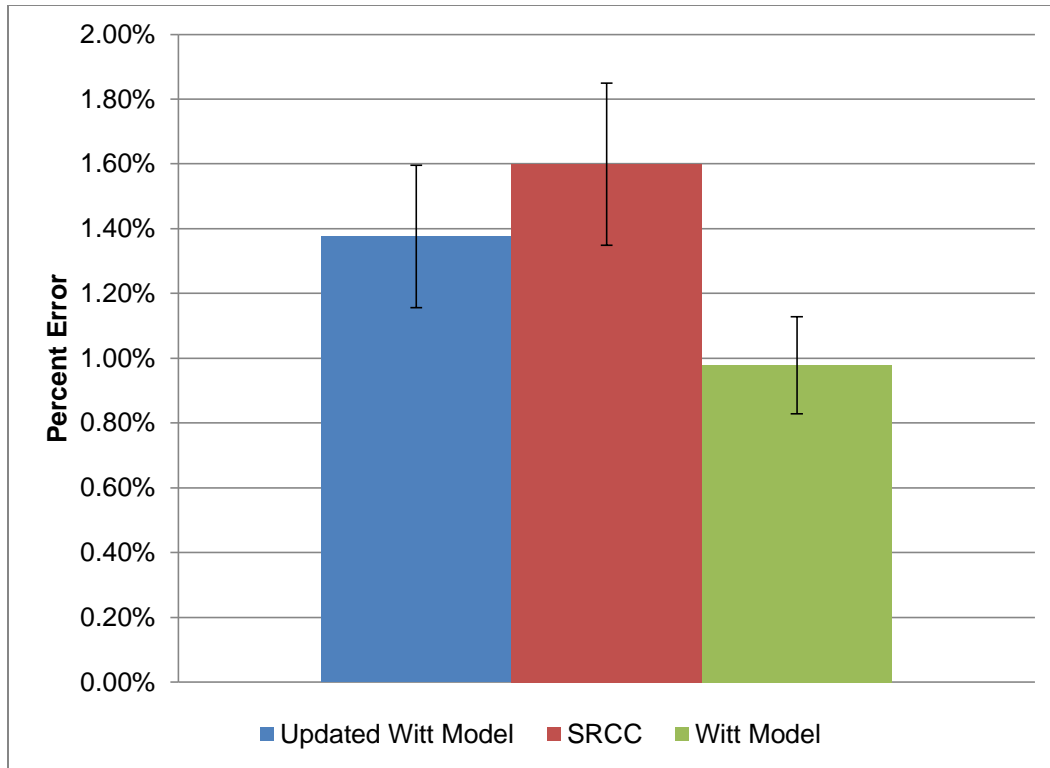
Figure 25. Percent error of each model for June 29th and June 30th tests

Table 5 shows the percent error calculated for each model. Based on the single row analysis, the original Witt model was the most accurate at calculating outlet temperatures from the collector array. This is an interesting result considering there was a major miscalculation present in the original Witt model. With all other variables equal, this error resulted in lower calculated temperatures when compared to the Updated Model and the SRCC curve. The more accurate predictions from the original Witt model seemed to be completely coincidental and reflected that the Updated Model and SRCC efficiency curve may slightly over-predict the performance of the collector array. The other possibility is that the collector array is not operating optimally and is therefore producing slightly lower temperatures than expected.

Table 5. Percent Error for the June 29th and June 30th tests

	June 29th Average	June 30th Average	Overall Average
Updated Witt Model	1.24%	1.52%	1.38%
SRCC	1.48%	1.72%	1.60%
Witt Model	0.95%	1.01%	0.98%

5.4 – Multiple Row Model Validation

Testing on two rows of Apricus AP-30 collectors was performed in late July to early August of 2011. After a re-analysis of shading on the array, it was determined that the daily test time could be expanded. Therefore, data was recorded between the hours of 10AM and 4PM for the multiple row experiments. To ensure that the recorded data was valid, a sample size of ten test days was taken and analyzed.

As discussed previously, the multiple row test was limited to two collector rows. This was to ensure that the heat dump was capable of keeping the working fluid from boiling during the experiments. For the multiple row tests, fluid flow was valved off for the last row of the array. This diverted all flow through the front and middle row. The data acquired from these tests was then compared to the values calculated by the two models and the SRCC efficiency curve.

Similar to the analysis done for the single row tests, the values predicted by each model were compared to the recorded temperature readings and a percent error was calculated. Figure 26 shows the overall average percent error for each model.
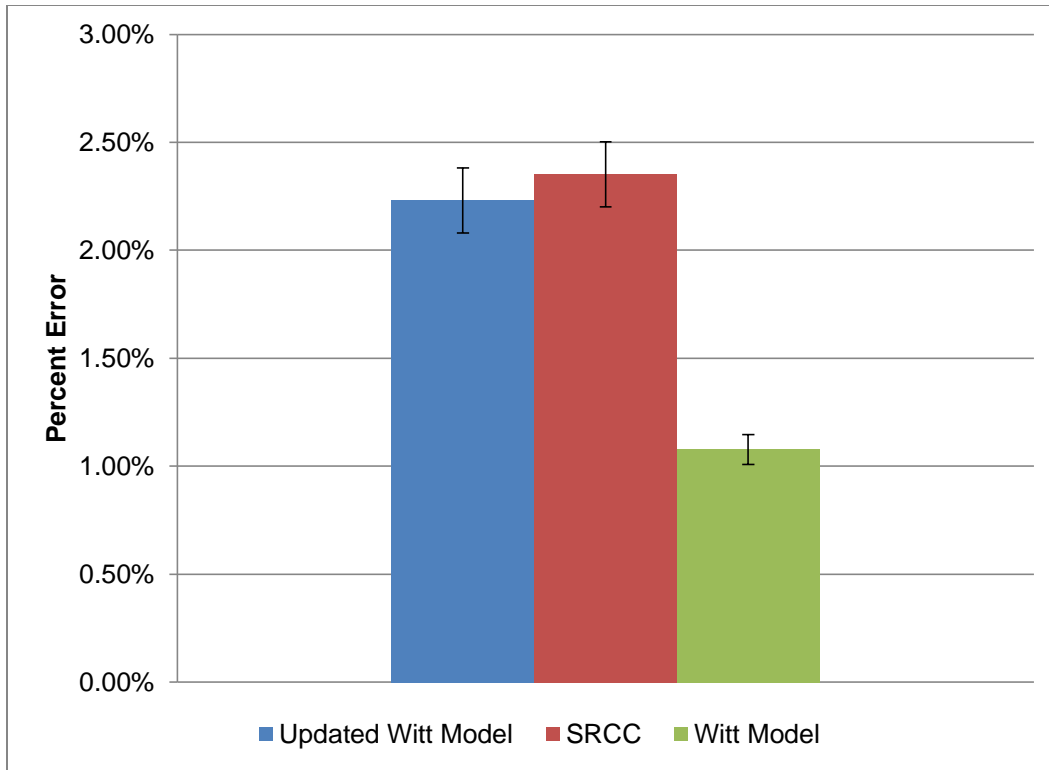
Figure 26. Percent error for multiple row tests

Table 6 shows the overall average percent error for the two models and the SRCC curve.

Table 6. Percent Error for multiple row tests

	Overall Average
Updated Witt Model	2.23%
SRCC	2.35%
Witt Model	1.08%

When comparing temperature values from each model, it was noted that the Witt model was again the most accurate at predicting the outlet temperatures of the array. It is also seen that the Updated Witt model and SRCC curve consistently gave higher values than what was actually recorded showing that some of the losses in the collector array were possibly not accounted for in these models. Therefore, the calculation error in the Witt model actually acts as a

47

partial replacement to some of the losses that were not introduced into the Updated Witt model and the SRCC curve.

5.5 – Storage Temperature Analysis

To determine the storage capability of this system, a program was added to the Updated Witt model to predict the fluid temperature in the storage container. Because this program was a late addition to the model, it was not validated through comparison to experimental data. However, data was still calculated with the program, and these results are shown below.

Figure 27 was created to show the predicted temperature of the storage container during the months of June and July. This was done to give a general view of how quickly the storage temperature builds. The starting temperature was set to 60°C, which is the expected outlet temperature of the DNEE under normal operating conditions [45]. Therefore, it was assumed that the storage temperature would not drop below this at any time during the night. The flow rate in the array during this analysis was set to 6 GPM since this is approximately where the system typically ran during testing. Since the model predicted that the array would have a positive output starting at 8 AM for both months, the analysis was started at that time. It should be noted that the analysis was stopped once the temperature of the fluid reached the boiling point. Since the system is at atmospheric pressure, the water in the storage container would just begin to boil off at this point, so it was decided to stop the analysis at this point.
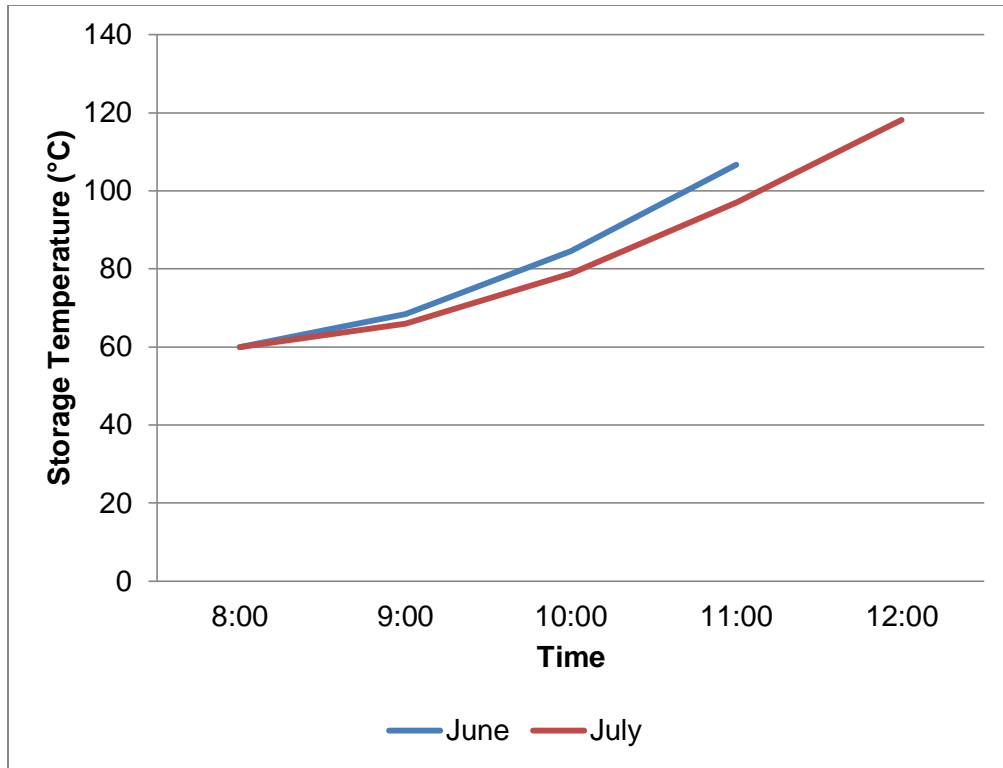
Figure 27. Predicted storage tank temperature for June and July

Figure 28 shows the predicted time for the water in the storage tank to reach the start of boiling at 100°C. For a normal day in June, the water in the storage tank would start boiling a little after 10:30 AM, which is two and a half hours after the start of the test. In July, this time would slightly over three hours. It should also be noted that the outlet temperature from the collector array reaches the boiling point well before the water in the storage container.
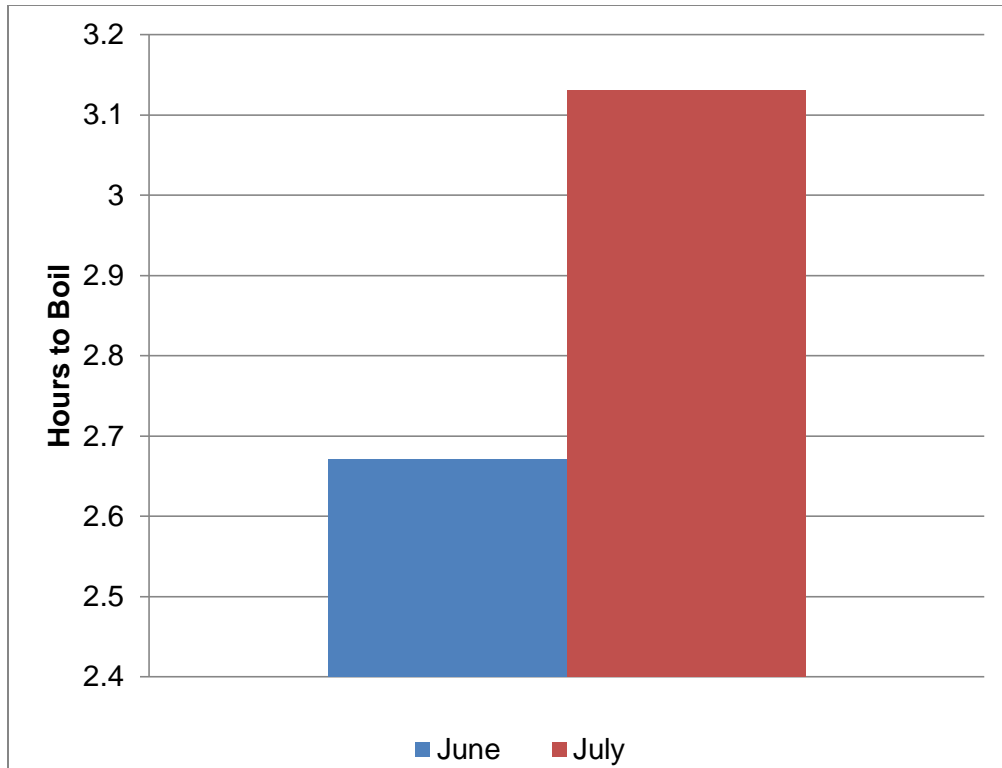
Figure 28. Time required for thermal storage to reach boiling point

5.6 – Storage Temperature Analysis with the DNEE Active

The storage temperature program in the Updated Witt model was also used to calculate the temperature of the storage tank throughout a typical day in June with the DNEE operating. Since the true amount of thermal energy needed to fully operate the DNEE was never determined in this project, the thermal input to the DNEE was calculated based on the design calculations made by Deluge Inc. [45]. Using information from previous engines, Deluge predicted that the engine in this project would operate at full capacity with 10 GPM of 180°F water. Introducing this assumption into equation 2, it was determined that the thermal load on the storage tank would be 28.78 kW.

Once the thermal load was determined, an analysis was done to determine the best size for the storage tank and collector array to operate the DNEE constantly during an entire June day. Based on the Updated Witt model, the collector performance is highest during the month of June, so it was selected as the month to optimize the system. From here, the number of collector rows and the size of the thermal storage was varied to ensure that the system could maintain a storage temperature above the inlet temperature of the DNEE while also staying below boiling at the hottest part of the day. It was important to stay above the inlet temperature of DNEE to ensure that the engine would be able to operate at full capacity at all times during the day running only on solar energy.

The size of the storage tank was determined by testing different masses of storage with the Updated Witt model. It was found that the temperature of the thermal storage changed too quickly at masses smaller than 10,000 kg. This leads to the fluid in the tank quickly reaching the boiling point during the hottest parts of the day and cooling off too quickly in the evening. Therefore, a storage size of 10,000 kg was chosen. This coverts to a volume of approximately 2700 gallons.

5.7 – Thermal Loss Analysis

The Updated Witt model can also be used to determine the points of highest thermal loss in the system. This information can then be used to determine the improvements that will most impact the performance of the collector array and associated thermal storage system. A brief analysis was done on the current configuration of the array to find the system losses at several points in the system. The analysis was done using the stored environmental data

for 1:00 PM during the month of June and included thermal loss calculations at
the manifold (Eq. 17), radiation losses at the absorber (Eq. 18), and at the
storage container (Eq. 19).

$$L_{ma} = \frac{(T_f - T_a)}{R_{ma}} A_{ma} \qquad [17]$$

$$L_{rad} = \frac{(T_{abs} - T_a)}{R_{rad}} A_{abs} \qquad [18]$$

$$L_s = (UA)_s (T_s - T_a) \qquad [19]$$

As seen in table 7, the radiative losses of the collector are the highest. This is not
totally surprising since the absorber plate is typically at the highest temperature
in the system.

Table 7. Calculated thermal loss in the Apricus AP-30 Collector

	Thermal Loss (W)
Storage	207
Manifold	67
Radiation	1611

5.7 – Summary

Each model was compared to the experimental results recorded during
June, July, and August. A percent error analysis was done comparing the
calculations from each model to the recorded outlet temperature of the collector
array. It was found that the original Witt model was the most consistently
accurate at predicting the outlet temperature value of the array with the Updated
Witt model being the next most accurate. The overall percent error for each
model can be seen in Table 8. This information includes the results from every
analysis listed in this section.

Table 8. Overall average percent error for each model

	Overall Average
Updated Witt Model	1.81%
SRCC	1.98%
Witt Model	1.03%

CHAPTER 6

RECOMMENDATIONS FOR FUTURE WORK AND CONCLUSIONS

6.1 – Recommendations for future work

Throughout the experiment, multiple opportunities to improve the collector array and the model developed. The major problem with the design of the array is the lack of insulation on the copper plumbing lines. Because of this short coming, significant heat loss occurs throughout the system before the fluid returns to the storage container. Insulation should also be added to the storage container. Adding a cheap insulation to the outside of the plumbing would result in a huge decrease in the thermal loss of the system.

Complete automation of the array control system would also be hugely beneficial. Designing a system that would automatically turn the system pump on once the collector array starts receiving solar radiation in the morning and turns the pump off once the array stops heating the fluid at night would increase the storage efficiency of the system. Also the heat dump could be maximized to fully remove the heat generated by all three rows of collectors.

Validation of the Updated model for the entire year would contribute to validity of the model. The testing and verification done in this experiment occurred during the summer. To have full confidence in the model, it must be tested and validated for the entire year. Other contributions could be made to the scope of the model. It could be adapted to easily analyze collectors in different locations other than Phoenix, AZ as well as different models of evacuated tube collectors. It would also be advantageous to test verify the model beyond two rows of collectors. In order to do this, a larger heat dump would have to be

developed, or a thermal load would have to be placed on the system during the summer months.

Several advancements to the Updated Witt model could also be made. This would involve expanding the model to include the ability to other heat transfer fluids other than water. The model could also be changed to calculate the performance of collectors other than the Apricus AP-30. Finally, to determine the true thermal value of the hot fluid coming from the collector array, an exergy analysis could be designed and integrated into the model. This would give an even better picture on the usefulness of the collector array.

6.2 – Conclusions

In this analysis, modifications were made to the Witt model to increase its ease of use and correct previous calculation errors. Through experimental validation, both models were found to generate accurate performance predictions for the Apricus AP-30 collector array. It was also found that the models consistently outperformed the SRCC efficiency curve at predicting the output of the array.

In order to verify the models discussed above, fifteen Apricus AP-30 collectors were laid out and built on the Arizona State University campus in Tempe, AZ. This analysis could also be considered a verification of the design of the collector array. Therefore, by comparing the output from the array to the externally verified model from SRCC, it was found that the collector array performs reasonably close to what is expected. Based on that result, it is determined that the array was properly designed and setup.

Though the ultimate goal of the collector array was to supply thermal energy to the Deluge Natural Energy Engine, performance problems with the engine during setup kept the two systems from being connected. The DNEE was operated using thermal energy from Rinnai tankless water heaters to ensure a consistent heat source. However, the engine was never able to operate at a level sufficient to produce measurable cooling from the air conditioning system. Several improvements to the design of the engine were made, but these only resulted in a slight increase in performance. To further increase the engine's output, the design of the heat exchanger will be changed from a tube in tube design to a shell and tube system. It is expected that this change will increase the engine's performance enough to begin generating cooling from the system.

Based on estimates from Deluge Inc., the collector array will only supply a small percentage of the thermal energy required to operate the DNEE. With the current footprint of the array calculated at approximately 90 m^2, an array that would completely supply the thermal energy to the DNEE would be very large, which would impact the feasibility of this system. However, the energy requirements of the DNEE will need to be experimentally verified prior to determining the proper collector array sizing.

REFERENCES

[1] U.S Department of Energy. "The History of Solar." [Online]. July 2011.
<http://www1.eere.energy.gov/solar/pdfs/solar_timeline.pdf>

[2] S.A Kalogirou, "Solar thermal collectors and applications," *Progress in Energy and Combustion Science* 30 (2004): 231-295.

[3] M. Witt, *Laboratory Simulation, Computer Modeling, and Design of a Solar Thermal Ammonia-Water Absorption Refrigeration System*. Tempe: Arizona State University, 2010.

[4] Deluge Incorporated. Deluge Products. [Online]. July 2011
<http://www.delugeinc.com/products.aspx>

[5] S.A. Klein and D.T. Reindl, "Solar Refrigeration," *ASHRAE Journal* 47 (2005) S26-S30.

[6] S.O. Enibe, "Solar Refrigeration for Rural Applications," *Renewable Energy* 12 (1997): 157-167. Print.

[7] J.A. Duffie and W.A. Beckman, *Solar Engineering of Thermal Processes*, Third Edition. New York: John Wiley, 2006.

[8] H. Wang et. al., "Performance of a combined organic Rankine cycle and vapor compression cycle for heat activated cooling," *Energy* 36 (2011): 447-458.

[9] R.I. Loehrke, "A passive, vapor-compression refrigerator for solar cooling," *Journal of Solar Energy Engineering*, vol. 112, pp. 191-195, 1990.

[10] M. Ohtsubo, H. Kasagi, K. Kashiwamura, and M. Sugihara, "The application of solar heating, cooling and hot water supply system with a Rankine cycle engine driven refrigerator for a small-sized building," *Solar Technology in the Eighties. Proceedings of the ISES Solar World Congress*, Brighton, UK, 1982, p. 526.

[11] N.M. Villar et. al., "Numerical 3-D heat flux simulations on flat plate solar collectors," *Solar Energy*, vol. 83, pp. 1086-1092, 2009.

[12] M. Selmi, M.J. Al-Khawaja, and A. Marafia, "Validation of CFD simulation for flat plate solar energy collector," *Renewable Energy*, vol. 33, pp. 383-387, 2008.

[13] S.A. Kalogirou, "Prediction of flat-plate collector performance parameters using artificial neural networks," *Solar Energy*, vol. 80, pp. 248-259, 2006.

[14] K.V. Karanth, M.S. Manjunath, and N.Y. Sharma, "Numerical Simulation of a Solar Flat Plate Collector using Discrete Transfer Radiation Model (DTRM) – A CFD Approach," *Proceedings of the World Congress on Engineering*, vol. III, 2011.

[15] W. Zima and P. Dziewa, "Modeling of liquid flat-plate solar collector operation in transient states," *Proceedings of the Institution of Mechanical Engineers, Part A: Journal of Power and Energy*, vol. 225, pp. 53-62, 2011.

[16] I. Budihardjo and G.L. Morrison. "Performance of water-in-glass evacuated tube solar water heaters," *Solar Energy*, vol. 83, pp. 49-56, 2009.

[17] Y. Kim and T. Seo, "Thermal performances comparisons of the glass evacuated tube solar collectors with shapes of absorber tube," *Renewable Energy*, vol. 32, pp. 772-795, 2007.

[18] N. Sharma and G. Diaz, "Performance model of a novel evacuated-tube solar collector based on minichannels," *Solar Energy*, vol. 85, pp. 881-890, 2011.

[19] X.R. Zhang and H. Yamaguchi, "An experimental study on evacuated tube solar collector using supercritical CO_2," *Applied Thermal Engineering*, vol. 28, pp. 1225-1233, 2008.

[20] K.C. Ng, C. Yap, and T. H. Khor, "Outdoor testing of evacuated-tube heat-pipe solar collectors," *Proceedings of the Institution of Mechanical Engineers,* vol. 214, pp. 23-30, 2000.

[21] Çengel, Yunus A. and Michael A. Boles, *Thermodynamics: An Engineering Approach*, Sixth Edition. New York: McGraw-Hill, 2008.

[22] B. Kongtragool and S. Wongwises, "A review of solar-powered Stirling engines and low temperature differential Stirling engines," *Renewable and Sustainable Energy Reviews,* vol. 7, pp. 131-154, 2003.

[23] Çengel, Yunus A., *Heat and Mass Transfer: A Practical Approach*, Third Edition. New York: McGraw-Hill, 2007.

[24] F-Chart Software, *Engineering Equation Solver*. Computer Program.

[25] Grundfos Pumps Corporation. (Accessed: July 2011) Technical Data. [Online]. http://www.us.grundfos.com/web/download.nsf/Pages/ CB0DD920244366288825650C0067D3BC/$File/L-UP-TL-107.PDF

[26] Rinnai Corporation. (Accessed: August 2011). [Online]. http://www.rinnai.us/documentation/downloads/R94LSe_SP_UC.pdf

[27] Amcot Cooling Towers Corporation. (Accessed: August 2011) Operating Instructions and Service Manual. [Online]. www.**amcot**.com/temp/**ST**_MANUAL.DOC

[28] Tranter Inc. (Recorded: August 2011) Heat Exchanger name plate.

[29] Apricus Solar Company Ltd. (Accessed: March 2011) Sustainable Hot Water Solutions. [Online]. <http://www.apricus.com/ >

[30] Onicon Incorporated. (Accessed: September 2011) F-1300 Series. [Online]. http://www.onicon.com/F1300.html

[31] Omega Engineering Inc. (Accessed: July 2011) Omega Products. [Online]. www.omega.com

[32] National Instruments Corporation. (Accessed: July 2011). National Instruments Products. [Online]. www.ni.com

[33] Slaman, M., and R. Griessen, "Solar Collector Overheating Protection," *Solar Energy,* vol. 83, pp. 982-987, 2009.

[34] Bi-Torq Valve Automation. (Accessed: July 2011) Bi-Torq Products. [Online]. www.bitorq.com

[35] Spectra Premium Industries. (Accessed: September 2011) eCatalog. [Online]. www.spectrapremium.com

[36] Intermatic Inc. (Recorded: September 2011) Automatic Pool Timer Information Sheet.

[37] Astrodyne Corporation. (Accessed: July 2011) Power Supplies. [Online]. www.astrodyne.com

[38] Compressor Works Inc. (Accessed: September 2011) Engine Cooling Products. [Online]. www.compressorworks.com/default.aspx

[39] Salt River Project. (Accessed: September 2011) "SRP Time-of-Use Price Plan". [Online]. <http://www.srpnet.com/prices/home/tou.aspx>

[40] University of Arizona. (Acessed: March 2011) Arizona Meteorological Network. <http://ag.arizona.edu/azmet/>

[41] Omega Engineering Inc. (Accessed: November 2011) 16-Channel Thermocouple Module. [Online]. http://sine.ni.com/ds/app/doc/p/id/ds-69/lang/en

[42] Omega Engineering Inc. (Accessed: November 2011) International Thermocouple Color Codes. [Online]. http://www.omega.com/techref/thermcolorcodes.html

[43] National Instruments Corporation. (Accessed: November 2011) Voltage Analog Input Module. [Online]. http://sine.ni.com/ds/app/doc/p/id/ds-190/lang/en

[44] Taylor, John R., *An Introduction to Error Analysis: The Study of Uncertainties in Physical Measurements*, Second Edition. Sausalito, CA: University Science Books, 1997.

[45] Brian Hageman, Deluge Inc., February 2011, Personal Conversation

[46] Solar Rating & Certification Corporation. (Accessed: September 2011) OG-100 Rating Directory. [Online]. <www.solar-rating.org>

.

APPENDIX A
SOLAR ENERGY COLLECTOR PROPERTIES

Solar energy collectors

Motion	Collector type	Absorber type	Concentration ratio	Indicative temperature range (°C)
Stationary	Flat plate collector (FPC)	Flat	1	30–80
	Evacuated tube collector (ETC)	Flat	1	50–200
	Compound parabolic collector (CPC)	Tubular	1–5	60–240
Single-axis tracking			5–15	60–300
	Linear Fresnel reflector (LFR)	Tubular	10–40	60–250
	Parabolic trough collector (PTC)	Tubular	15–45	60–300
	Cylindrical trough collector (CTC)	Tubular	10–50	60–300
Two-axes tracking	Parabolic dish reflector (PDR)	Point	100–1000	100–500
	Heliostat field collector (HFC)	Point	100–1500	150–2000

Note: Concentration ratio is defined as the aperture area divided by the receiver/absorber area of the collector.

Figure A.1. Solar Collector Properties [7]

APPENDIX B

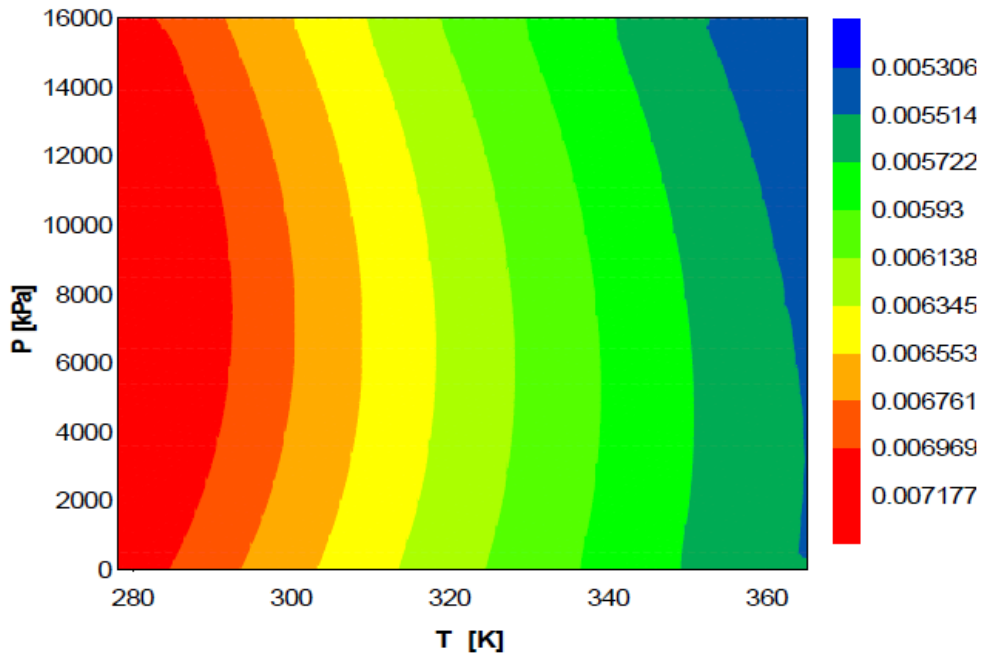3-D PLOTS OF THERMAL EXPANSION CAPABILITIES OF FLUIDS [β/c_p] [24]

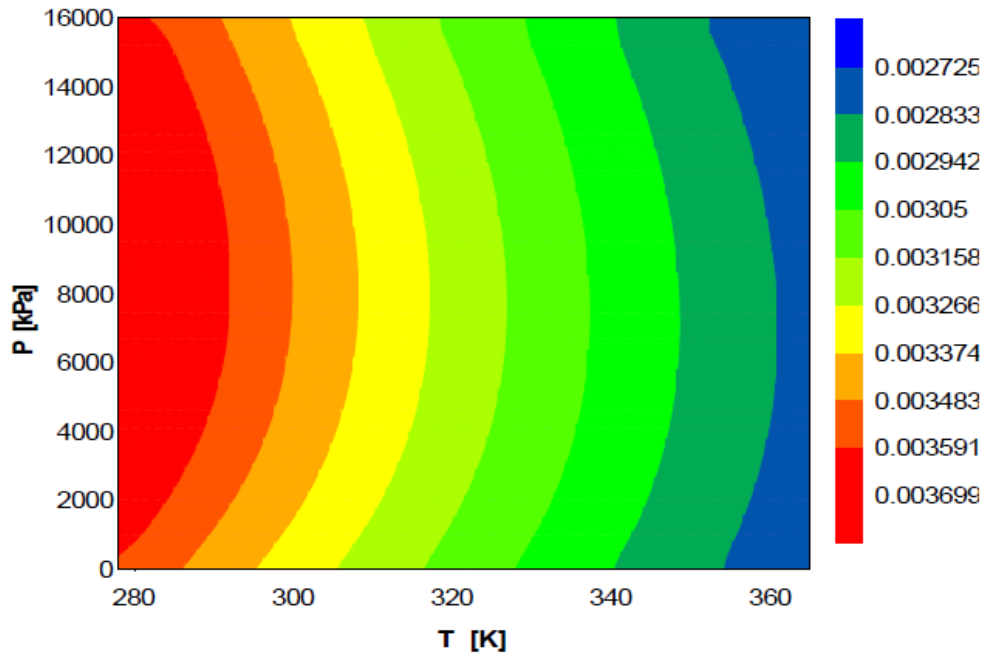Figure B.1 Ratio plot of thermal expansion over specific heat for Argon

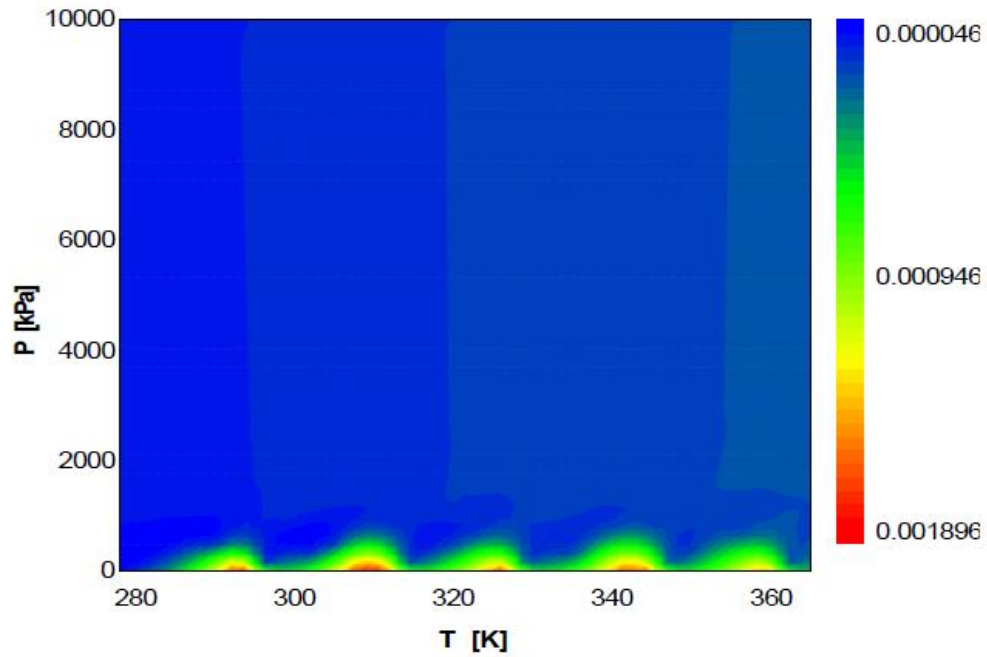Figure B.2 Ratio plot of thermal expansion over specific heat for CO

Figure B.3 Ratio plot of thermal expansion over specific heat for Water
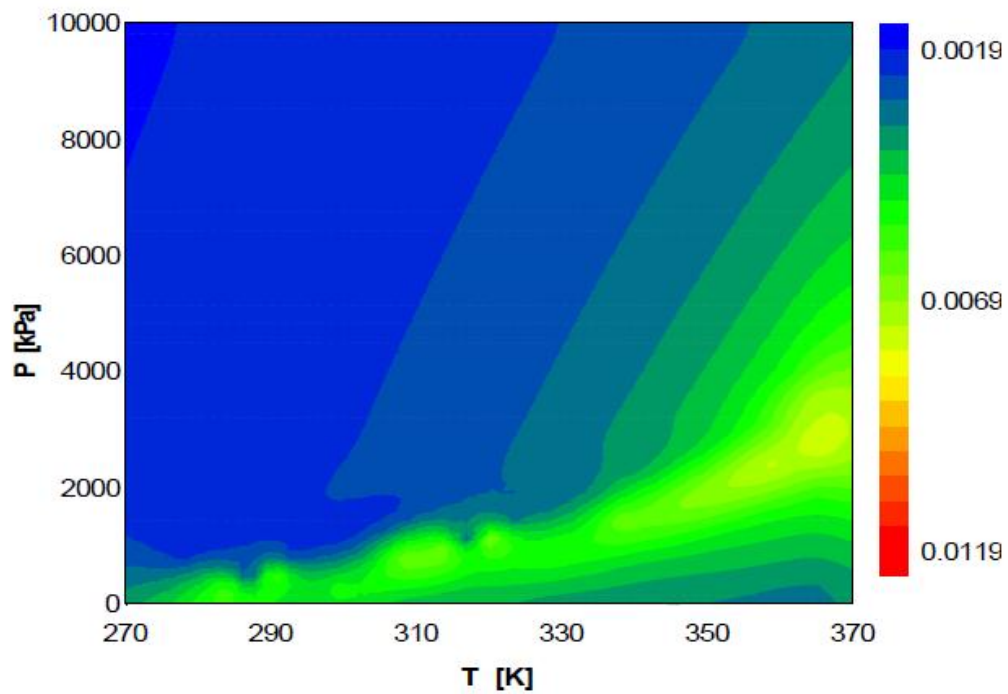
Figure B.4 Ratio plot of thermal expansion over specific heat for R134-a
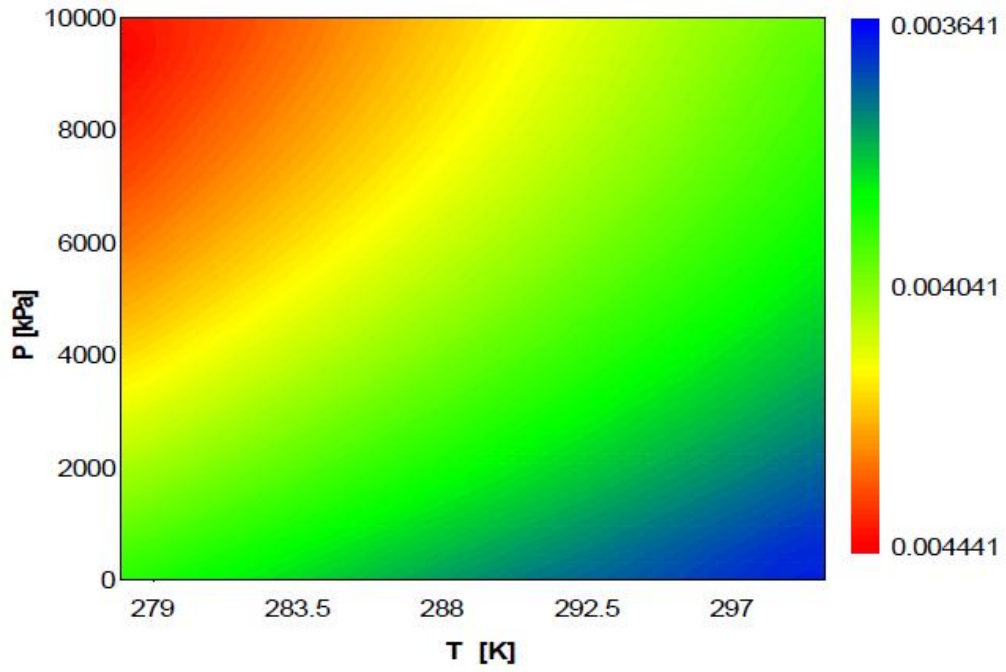
Figure B.5 Ratio plot of thermal expansion over specific heat for Oxygen

APPENDIX C

PUMP CURVE FOR THE GRUNDFOS UPS SERIES PUMPS [25]

Pump performance curves

Curve	Pump
1.	UP 26-99 F
2.	UP 43-75 F
3.	UP 26-96 F
4.	UP 26-64 F
5.	UP 15-42 F BRUTE II
6.	UP 15-42 FC
7.	UPS 15-42 F SPD. 3
8.	UPS 15-42 F SPD. 2
9.	UPS 15-42 F SPD. 1
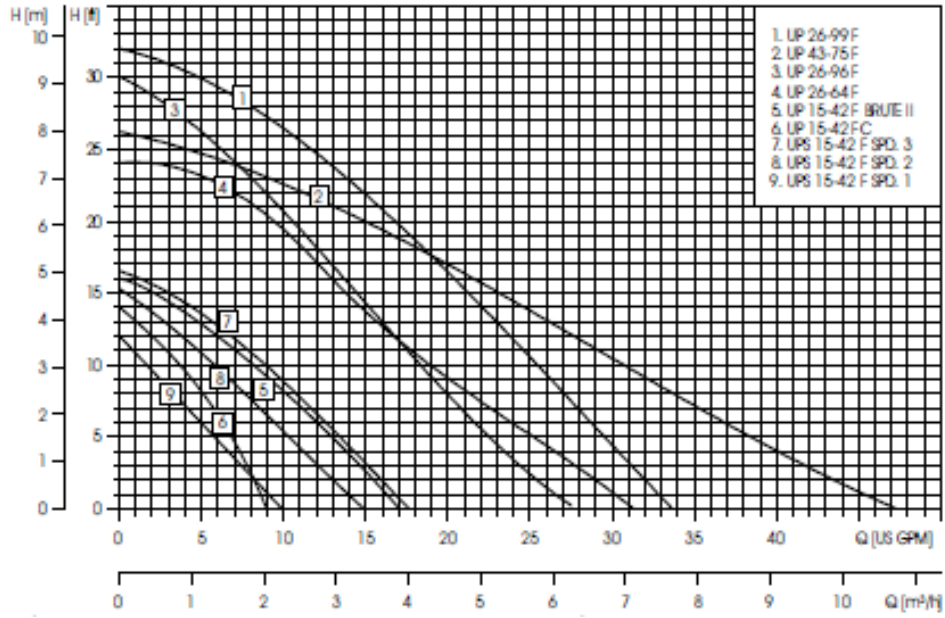
APPENDIX D

APRICUS AP-30 COLLECTOR SRCC CERTIFICATION

SOLAR COLLECTOR CERTIFICATION AND RATING	CERTIFIED SOLAR COLLECTOR
SRCC OG-100 CERTIFIED SRCC OG-100	SUPPLIER: Apricus Inc. 6 Sycamore Way, Unit #2 Branford, CT 06405 USA MODEL: Apricus AP-30 COLLECTOR TYPE: Tubular CERTIFICATION#: 2007033A

COLLECTOR THERMAL PERFORMANCE RATING

	Kilowatt-hours Per Panel Per Day				Thousands of BTU Per Panel Per Day			
CATEGORY (Ti-Ta)	CLEAR DAY	MILDLY CLOUDY	CLOUDY DAY	CATEGORY (Ti-Ta)	CLEAR DAY	MILDLY CLOUDY	CLOUDY DAY
A (-5 °C)	13.5	10.2	6.9	A (-9 °F)	46.1	34.8	23.5
B (5 °C)	12.9	9.6	6.3	B (9 °F)	44.0	32.7	21.4
C (20 °C)	11.9	8.6	5.3	C (36 °F)	40.6	29.3	18.0
D (50 °C)	10.0	6.7	3.5	D (90 °F)	34.2	23.0	11.8
E (80 °C)	7.9	4.7	1.7	E (144 °F)	27.1	15.9	5.9

A- Pool Heating (Warm Climate) B- Pool Heating (Cool Climate) C- Water Heating (Warm Climate) D- Water Heating (Cool Climate) E- Air Conditioning

Original Certification Date: 24-AUG-09

COLLECTOR SPECIFICATIONS

Gross Area: 4.158 m²   44.76 ft² Net Aperture Area: 2.98 m² 32.05 ft²
Dry Weight: 96.2 kg   212. lb Fluid Capacity: 1.0 liter 0.3 gal
Test Pressure: 1103. KPa   160. psig

COLLECTOR MATERIALS

Frame: Stainless Steel
Cover (Outer): Glass Vacuum Tube
Cover (Inner): None

Pressure Drop

Flow		ΔP	
ml/s	gpm	Pa	In H₂O
20.00	0.32	105.00	0.42
50.00	0.79	524.0	2.1
80.00	1.27	1257.00	5.05

Absorber Material: Tube - Copper / Plate - Aluminum   Insulation Side: Vacuum

Absorber Coating: Aluminum Nitride   Insulation Back: Vacuum

TECHNICAL INFORMATION

Efficiency Equation [NOTE: Based on gross area and (P)=Ti-Ta]   Y INTERCEPT   SLOPE

SI Units: $\eta = 0.456 \quad -1.35090\ (P)/I \quad -0.00381\ (P)^2/I$ 0.458   -1.579 W/m²·°C

IP Units: $\eta = 0.456 \quad -0.23796\ (P)/I \quad -0.00037\ (P)^2/I$ 0.458   -0.278 Btu/hr·ft²·°F

Incident Angle Modifier [[$(S)=1/\cos\theta - 1$, $0° < \theta <= 60°$]

K$_{\tau\alpha}$ = 1 $1.306\ (S) \quad -1.034\ (S)^2$ Test Fluid: Water

K$_{\tau\alpha}$ = 1 $0.23\ (S)$ Linear Fit   Test Flow Rate: 20.0 ml/s·m²   0.0294 gpm/ft²

REMARKS: Tested with long axis of tubes oriented north-south. IAM perpendicular to the tubes is listed above. IAM parallel to the tubes = 1.0 - 0.09(S)

October, 2011
Certification must be renewed annually, For current status contact:
SOLAR RATING & CERTIFICATION CORPORATION
400 High Point Drive, Suite 400 ♦ Cocoa, Florida 32926 ♦ (321) 213-6037 ♦ Fax (321) 821-0910

Figure D.1. SRCC Certification for the Apricus AP-30 Collector [46]

APPENDIX E

APRICUS AP-30 SPECIFICATIONS [29]

Apricus Solar Collector General Specifications

Manifold Casing Material	Aluminum (grade 3A21)
Frame Material	1.5mm 304 Stainless Steel
Header Pipe Material	99.93% pure Copper & lead free 45% silver brazing
Insulation	Compressed Glass Wool - K = 0.043W/mK
Rubber Seals and Rings	HTV grade silicone rubber
Optimal installation angle	20-70° Vertical, -5° to +5° Horizontal
Maximum Operating Pressure	8bar - 116psi
Optimal flow rate	0.1L/min/tube - 0.026G/min/tube
Performance Data (SPF)	Conversion Factor: ho = 0.717 Loss Coefficients: a1 = 1.52, a2 = 0.0085

Model Specifications

Model	AP-Demo	AP-10	AP-20	AP-22	AP-30
Overall Length (mm / inch) 1	660 / 25.9"	1980 / 77.9"			
Overall Width (mm / inch)	376 / 14.8"	796 / 31.3"	1496 / 58.8"	1636 / 64.4"	2196 / 86.4"
Overall Height (mm / inch)	156 / 6.1" (including flush roof mounting frame)				
Absorber Area (m^2 / ft^2) 2	0.08 / 0.86	0.8 / 8.6	1.6 / 17.2	1.76 / 18.9	2.4 / 25.8
Fluid Capacity (ml / ounces)	190 / 6.4	290 / 9.8	510 / 17.2	550 / 18.6	833 / 28.2
Gross Area (m^2 / ft^2) 3	0.25 / 2.67	1.57 / 16.95	2.96 / 31.8	3.24 / 34.8	4.35 / 46.8
Dry Weight (kg / pounds)	8 / 18	35 / 77	64 / 140	71 / 157	95 / 209